Modeling long-term fire impact on ecosystem characteristics and surface energy using a process-based vegetation-fire model SSiB4/TRIFFID-Fire v1.0

Huilin Huang[1], Yongkang Xue[1, 2], Fang Li[3], and Ye Liu[1]

5   1. Department of Geography, University of California, Los Angeles, CA 90095, USA

2. Department of Atmospheric & Oceanic Sciences, University of California, Los Angeles, CA 90095, USA

3. International Center for Climate and Environmental Sciences, Institute of Atmospheric Physics, Chinese Academy of Sciences, Beijing, China

10   Correspondence to: Yongkang Xue (yxue@geog.ucla.edu)

Abstract

15    Fire is one of the primary disturbances to the distribution and ecological properties of the world's major biomes and can influence the surface fluxes and climate through vegetation-climate interactions. This study incorporates a fire model of intermediate complexity to a biophysical model with dynamic vegetation, SSiB4/TRIFFID (The Simplified Simple Biosphere Model coupled with the Top-down Representation of Interactive Foliage and Flora Including Dynamics

20 Model). This new model, SSiB4/TRIFFID-Fire, updating fire impact on the terrestrial carbon cycle every 10 days, is then used to simulate the burned area during 1948-2014. The simulated global burned area in 2000-2014 is 471.9 Mha yr^{-1}, close to the estimate, 478.1 Mha yr^{-1}, in Global Fire Emission Database v4s (GFED4s) with a spatial correlation of 0.8. The SSiB4/TRIFFID-Fire reproduces temporal variations of the burned area at monthly to interannual scales. Specifically, it

25 captures the observed decline trend in northern African savanna fire and accurately simulates the fire seasonality in most major fire regions. The simulated fire carbon emission is 2.19 Pg yr^{-1}, slightly higher than the GFED4s (2.07 Pg yr^{-1}).

    The SSiB4/TRIFFID-Fire is applied to assess the long-term fire impact on ecosystem characteristics and surface energy budget by comparing model runs with and without fire (FIRE-

30 ON minus FIRE-OFF). The FIRE-ON simulation reduces tree cover over 4.5 % of the global land surface, accompanied by a decrease in leaf area index and vegetation height by 0.10 m^2 m^{-2} and 1.24 m, respectively. The surface albedo and sensible heat are reduced throughout the year, while latent heat flux decreases in the fire season but increases in the rainy season. Fire results in an increase in surface temperature over most fire regions.

1. Introduction

Wildfire, whether natural or human-made, is one of the primary ecosystem disturbances and it plays a major role in the terrestrial biogeochemical cycles and ecological succession across spatial and temporal scales (Sousa, 1984; Bowman et al., 2009). Every year in the dry season, wildfires burn about 400 Mha of land vegetated areas, leaving behind numerous scars in the landscape (Giglio et al., 2013; Chuvieco et al., 2016). Fires affect the climate through modification of water, energy, and momentum exchange between land and atmosphere (Chambers and Chapin, 2002; Bond-Lamberty et al., 2009) and can interact with monsoons by affecting atmospheric circulations (De Sales et al., 2016; Saha et al., 2016). Fires are also important sources of global carbon, aerosols, and trace gas emissions. Based on the latest satellite estimates, global fires emit $1.5 - 4.2$ Pg C yr^{-1} carbon, $7 - 8.2$ Pg C yr^{-1} CO_2, and $1.9 - 6.0$ Tg C yr^{-1} black carbon to the atmosphere (Chuvieco et al., 2016; van der Werf et al., 2017; Li et al., 2019). Fire emissions contribute to increases in greenhouse gases and cloud condensation nuclei through geochemistry processes (Scholes et al., 1996), affecting radiative forcing, the hydrology cycle (Ward et al., 2012; Jiang et al., 2016; Hamilton et al., 2018), and air quality (van der Werf et al., 2010; Johnston et al., 2012).

Since the early 2000s, fire models have been developed within Dynamic Global Vegetation Models (DGVMs) to explicitly describe the burned area, fire emissions, and fire disturbance on terrestrial ecosystems (Thonicke et al., 2001; Venevsky et al., 2002; Arora and Boer, 2005; Thonicke et al., 2010; Li et al., 2012; Pfeiffer et al., 2013; Lasslop et al., 2014; Yue et al., 2014; Rabin et al., 2018; Burton et al., 2019; Venevsky et al., 2019). These fire models have various levels of complexity, from simple statistical models (SIMFIRE; Knorr et al., 2016) to complicated process-based ones such as SPITFIRE (Thonicke et al., 2010) and MC2 (Bachelet et al., 2015).

With increasing complexity, more fire processes and fire characteristics are considered in fire models. In general, current fire models broadly capture the global amounts and spatial distribution

60   of burned area and carbon emissions, as compared to different observations. However, many empirically determined parameters are included in the complicated process-based models, which leads to large uncertainties. There is no model that outperforms other models across all fire variables (Hantson et al., 2020). Moreover, current fire models have deficiencies in simulating the peak fire month, fire season length, and interannual variability, as reported by the Fire Model

65   Intercomparison Project (FireMIP; Hantson et al., 2020; Li et al., 2019). Most fire models show a 1-2 months shift in peak burned area and simulate a longer fire season compared to observations.

Fire models have been used to reconstruct fire history before the satellite era (Yang et al., 2015; van Marle et al., 2017; Li et al., 2019). In addition, they are widely used to attribute historical variability of burned area to various climate and anthropogenic driving factors (Kloster et al., 2012;

70   Andela et al., 2017; Forkel et al., 2019; Teckentrup et al., 2019). Some fire models have been used to assess long-term fire impact on the terrestrial carbon cycle by comparing a reference simulation with fire and a sensitivity simulation representing "a world without fire." However, the simulated responses of vegetation and carbon cycle are divergent. Bond et al. (2005) reported that forest cover would double in a world without fire, while in the recent fire-coupled DGVMs, a much

75   smaller tree cover reduction by 10% (ranges between 3 % and 25 %) is simulated when fire is taken into account (Lasslop et al., 2020). Earlier model-based studies reported that fire reduced terrestrial carbon uptake. However, the range of the quantified reduction was fairly broad (0.05–3.60 Pg C yr^{-1}), and most studies did not consider the fire effects on vegetation distribution and related mechanisms (Li et al., 2014; Yue et al., 2015; Poulter et al., 2015; Yang et al., 2015; Seo

80   and Kim, 2019; Zou et al. 2020).

Thus far, only the fire model developed by Li et al. (2012; 2013) has been used to investigate the long-term fire effects on surface energy. By comparing the simulated climate with and without fire, Li et al. (2017) concluded that fire caused a significant decrease in surface radiation, latent heat, and a slight decrease in sensible heat fluxes through changes in biophysical properties such as albedo, Bowen ratio, and aerodynamic resistance. An increase in surface temperature was found over most fire regions. However, the long-term fire impact on vegetation distribution was not taken into account in Li et al. (2017), which has been widely observed on site-level studies (Higgins et al., 2007; Smit et al., 2010) and can cause substantial changes in aerodynamic resistance due to conversions of dominant PFT (Huang et al. 2020). Moreover, Li et al. (2017) focused on the annual fire impact on energy fluxes. Yet fire effects on energy budget can have large seasonal variations associated with the vegetation loss during the fire seasons and vegetation recovery during post-fire rainy seasons. The seasonal variations in fire effects have not been investigated in any fire studies.

In the original SSiB4/TRIFFID, the carbon disturbance caused by fire and insects was assumed to be a constant which depended solely on plant functional type (PFT) without spatial and temporal changes (Cox et al., 2001; Liu et al., 2019). However, the fire disturbance is highly varied with climate, vegetation productivity, and socio-economic conditions, which has a strong influence on vegetation dynamics, carbon cycling, and soil processes. In this study, we develop the fire modeling by incorporating the fire scheme of Li et al. (2012; 2013) to SSiB4/TRIFFID (hereafter SSiB4/TRIFFID-Fire). The SSiB4/TRIFFID-Fire model updates fire-induced carbon loss every 10 days, which has been rarely employed in current process-based fire models, and is used to provide a quantitative assessment of fire impact on ecosystem characteristics and surface energy at subseasonal, seasonal, interannual, and long-term scales. Specifically, our objectives are:

(1) to evaluate the climatology and interannual variability of burned area and carbon emissions simulated by offline SSiB4/TRIFFID-Fire; (2) to assess the ability of SSiB4/TRIFFID-Fire in capturing the fire seasonality in major fire regions; and (3) to assess the long-term fire impact on PFT distribution and vegetation properties and the resultant changes in seasonal surface energy budget and temperature. In Sect. 2, we provide a brief description of the DGVM, SSiB4/TRIFFID, and the fire model, Li et al. (2012; 2013), and the coupling procedures. The experimental design and data for model input and validation are introduced in Sect. 3. The fire model evaluation on the global scale and the application of long-term fire impact on the ecosystem characteristics and surface properties are presented in Sect. 4. Discussions and conclusions are given in Sect. 5.

2. Method

2.1 Land and vegetation model

The Simplified Simple Biosphere Model (SSiB, Xue et al., 1991; Zhan et al., 2003) is a biophysical model which simulates fluxes of surface radiation, momentum, sensible/latent heat, runoff, soil moisture, surface temperature, and vegetation gross/net primary productivity (GPP/NPP) based on energy and water balance. The SSiB was coupled with a dynamic vegetation model, the Top-down Representation of Interactive Foliage and Flora Including Dynamics Model (TRIFFID), to calculate leaf area index (LAI), canopy height, and PFT fractional coverage according to the carbon balance (Cox, 2001; Zhang et al., 2015; Harper et al., 2016; Liu et al., 2019). We have improved the PFT competition strategy and plant physiology processes to make the SSiB4/TRIFFID suitable for seasonal, interannual, and decadal studies (Zhang et al., 2015; Liu et al., 2019). SSiB4/TRIFFID includes seven PFTs: (1) broadleaf evergreen trees (BET), (2) needleleaf evergreen trees (NET), (3) broadleaf deciduous trees (BDT), (4) C3 grasses, (5) C4 plants, (6) shrubs, and (7) tundra. The coverage of a PFT is determined by net carbon availability,

competition between species, and disturbance, which implicitly includes mortality due to fires, pests, and windthrow. A detailed description and validation of SSiB4/TRIFFID can be found in Zhang et al. (2015) and Liu et al. (2019).

2.2 Fire model and modifications

In this study, a process-based fire model of intermediate complexity has been implemented in the SSiB4/TRIFFID, called SSiB4/TRIFFID-Fire. The fire model developed by Li et al. (2012; 2013) was first built on the model platform of CLM-DGVM, and has been incorporated in IAP-DGVM (Zeng et al., 2014), CLM4.5 (Oleson et al., 2013), CLM5 (Lawrence et al., 2019), LM3 in Earth system model GFDL-ESM (Rabin et al., 2018; Ward et al., 2018), AVIM in Climate System Model BCC-CSM (W. P. Li, personal comm.), E3SM Land Model (ELM; Ricciuto et al., 2018), NASA GEOS catchment-CN4.5 model (Zeng et al., 2019), and DLEM (Yang et al., 2014), and partly used in GLASS-CTEM (Melton and Arora, 2016). The following briefly describes the fire schemes adapted from Li et al. (2012; 2013) and Li and Lawrence (2017) and our modifications.

The fire model comprises three parts: fire occurrence, fire spread, and fire impact. The basic equation is that the burned area in a grid cell (A_b, km^2 s^{-1}) is determined by the number of fires per time step (N_f, count s^{-1}) and the average spread area per fire (a, km^2 count^{-1}):

$$A_b = N_f a. \tag{1}$$

2.2.1 Fire occurrence

N_f is the product of the number of potential ignition counts due to both natural causes (I_n, count s^{-1} km^{-2}) and human ignitions (I_a, count s^{-1} km^{-2}), fuel availability (f_b), fuel combustibility (f_m), and human suppression factor (f_{eo}). In this paper, we only consider non-crop fire by excluding the cropland fraction (f_{crop}) from burning:

$$N_f = (I_n + I_a) f_b f_m f_{eo} (1 - f_{crop}) A_g, \tag{2}$$

150 where A_g is the land area of the grid cell (km^2). Fires in the croplands are excluded here due to their small extent within the major fire regions and their relatively low intensity (Bistinas et al., 2014). Cropland fire is still a major uncertainty in remote sensing datasets (Randerson et al., 2012), and more data and investigation are needed.

The number of natural ignitions is related to lightning flashes (I_l, count s^{-1}), cloud-to-

155 ground lightning fraction, $\frac{1}{5.16+2.16 \cos [3,min(60,\lambda)]}$, which depends on latitude λ (Prentice and Mackerras, 1977), and ignition efficiency (ψ = 0.22). The anthropogenic ignition, I_a, is parameterized using the number of potential anthropogenic ignitions by a person ($\alpha = 1.35 \times 10^{-9}$ count per person s^{-1}) and population density (D_p; person) (Venevsky et al. 2002):

$$I_n = \frac{\psi}{5.16+2.16 \cos [3,min(60,\lambda)]} I_l, \tag{3}$$

160 $$I_a = \alpha D_p \times (6.8 D_p^{-0.6}). \tag{4}$$

The fuel availability f_b (fraction, range 0−1) is given as:

$$f_b = \begin{cases} 0 & B_{ag} \leq B_{low} \\ \frac{B_{ag}-B_{low}}{B_{up}-B_{low}} & B_{low} < B_{ag} < B_{up}, \\ 1 & B_{ag} \geq B_{up} \end{cases} \tag{5}$$

where B_{ag} (g C m^{-2}) is the aboveground biomass (leaf and stem in SSiB4/TRIFFID-Fire) of all PFTs. Following Li et al. (2012), we use B_{low} = 155 g C m^{-2} as the lower fuel threshold, below

165 which fire does not occur and B_{up} = 1050 g C m^{-2} as the upper fuel threshold, above which fuel load is not a constraint for fire occurrence.

Fuel combustibility f_m (fraction, 0−1) is given as:

$$f_m = f_{RH} f_\theta, \tag{6}$$

where f_{RH} and f_θ represent the dependence of fuel combustibility on relative humidity (RH; %)

170 and the root zone soil moisture (θ), respectively (Li and Lawrence, 2017). Following Li et al.

(2013), we assume $f_m = 0$ when surface air temperature T is below -10 °C. f_{RH} reflects the impact of real-time climate conditions on fuel combustibility while f_θ reflects the response of fuel combustibility to the preceding climate conditions (Shinoda and Yamaguchi, 2003):

$$f_{RH} = \begin{cases} 0 & RH \geq RH_{up} \\ (\frac{RH_{up}-RH}{RH_{up}-RH_{low}})^{1.3} & RH_{low} < RH < RH_{up}, \\ 1 & RH \leq RH_{low} \end{cases} \tag{7}$$

$$f_\theta = \begin{cases} 0 & \theta \geq \theta_{up} \\ (\frac{\theta_{up}-\theta}{\theta_{up}-\theta_{low}})^{0.7} & \theta_{low} < \theta < \theta_{up}. \\ 1 & \theta \leq \theta_{low} \end{cases} \tag{8}$$

Relative humidity suppresses fire occurrence when it is larger than $RH_{up} = 70$ %, and relative humidity does not constrain fire when it is smaller than $RH_{low} = 30$ %. The PFT-dependent θ_{up} and θ_{low} are used as the upper and lower thresholds of soil moisture in a similar way as the thresholds of relative humidity (Table. 1). In Li fire scheme, this factor (f_θ) is parameterized using root-zone soil moisture potential factor β (0-1.0), a model-dependent variable used to calculate transpiration in CLM (Li and Lawrence 2017). β_{low}=0.85 and β_{up}=0.98 are used as the lower and upper thresholds for all PFTs, yet the narrow range of β in CLM5 has led to fire model too sensitive to drought. In SSiB4/TRIFFID-Fire, the root-zone soil moisture θ is found to be the best variable to describe the dependence of fuel combustibility on the preceding climate.

Table 1. The upper (θ_{up}) and lower (θ_{low}) thresholds of root zone soil moisture for PFTs in SSiB4/TRIFFID-Fire

Vegetation Types	θ_{up}	θ_{low}
BET	0.80	0.30
NET	0.80	0.30
BDT	0.80	0.30
C3 grasses	0.75	0.30
C4 plants	0.75	0.30

Shrubs	0.60	0.30
Tundra	0.60	0.30

The human suppression factor (f_{eo}; 0-1) reflects the demographic (f_d) and economic (f_e) impact on fire occurrence in populated areas (population density $D_p > 0.1$ per person km^{-2}):

190 $$f_{seo} = f_d f_e. \tag{9}$$

The human suppression is assumed to be negligible (f_{seo}=1) when $D_p \leq 0.1$ person km^{-2}. A detailed description of f_d and f_e parameterization can be found in Li et al. (2012; 2013).

2.2.2 Average spread area after fire ignition

The average spread area of a fire is assumed elliptical in shape with the ignition point

195 located at one of the foci and the fastest spread occurring along the major axis. The average burned area of a fire a (km^2 per count) is represented as (Li et al., 2012):

$$a = \pi L_B (u_{max} g_0 F_m \tau / 1000)^2 F_{se}, \tag{10}$$

where L_B is the length-to-breadth ratio of the ellipse shape and is related to the wind speed, W (m s^{-1}):

200 $$L_B = 1.0 + 10.0[1 - \exp(-0.06W)]. \tag{11}$$

u_{max} is the PFT-dependent maximum fire spread rate (m s^{-1}; Table S1); $g_0 = 0.05$ is the dependence of fire spread rate perpendicular to the wind direction; F_m is the influence of fuel wetness on fire spread and is assumed to be related to f_m in the fire occurrence Eq. (6):

$$F_m = f_m^{0.5}. \tag{12}$$

205 τ (=3600*24 s) is the global average fire duration, which is simply taken to be one day as reported by Giglio et al. (2006). The human suppression factor, F_{se}, reflects the human impact on fire spread through fire-fighting activities and is parameterized following Li et al. (2013).

2.2.3 Carbon emissions, post-fire mortality, and emissions of aerosols and trace gases

In post-fire regions, the fire carbon emission, φ_j (g C s^{-1}), from the vegetation tissue (leaf,

210   stem, root) of the jth PFT is calculated based on the burned area (A_b; km^2 s^{-1}):

$$\varphi_j = A_b \boldsymbol{C_j} \cdot \boldsymbol{CC_j}. \tag{13}$$

$\boldsymbol{C_j} = (C_{leaf}, C_{stem}, C_{root}, C_{litter})$ is carbon density vector (g C km^{-2}) for leaf, stem, root, and litter

of the jth PFT calculated in TRIFFID. As the carbon cycle in current SSiB4/TRIFFID does not

explicitly represent the litter carbon storage and decomposition, we assume the litter carbon and

215   woody debris account for about 25% of aboveground biomass for global forest and about 30% for

savanna/grassland based on previous studies (Pan et al., 2011; de Oliveira et al., 2019). $\boldsymbol{CC_j}$ is the

corresponding combustion completeness for leaf, stem, root, and litter of the jth PFT (Table S2).

Meanwhile, fire-induced mortality transfers carbon from uncombusted leaf, stem, and root to litter:

$$\psi_j = A_b \boldsymbol{C_j} \cdot (1 - \boldsymbol{CC_j}) \cdot \boldsymbol{M_j}, \tag{14}$$

220   where $\boldsymbol{M_j} = (M_{leaf}, M_{stem}, M_{root})$ is the corresponding mortality factor (Table S2).

Finally, the emissions of trace gases and aerosols species x for the jth PFT ($EM_{x,j}$, g s^{-1})

can be calculated from carbon emissions (φ_j) using the PFT-dependent emission factor ($EF_{x,j}$, g

species (kg dm)$^{-1}$):

$$EM_{x,j} = EF_{x,j} \frac{\varphi_j}{[C]}, \tag{15}$$

225   where $[C]$ (= 0.5 g C (kg dm)$^{-1}$) is a unit conversion factor from dry matter to carbon (Li et al.,

2019). The emission factors, $EF_{x,j}$, of trace gases and aerosols in Table S3 are based on Andreae

(2019). The emissions of trace gases and aerosols can be applied in the atmospheric chemistry

model to calculate the production of secondary aerosols, transport of pollutants, and the resultant

aerosol direct and indirect effects on climate.

2.2.4 Including the fire effect on the carbon pool

When Li et al. fire model is coupled with CLM, the vegetation distribution is prescribed using satellite-based land cover, and therefore the fire impact on vegetation cover is not simulated. In SSiB4/TRIFFID-Fire, the fire-related carbon loss due to combustion and post-fire mortality is transferred to changes of PFT fraction based on carbon balance.

In TRIFFID (Cox, 2001), the fractional change of the jth PFT ($\frac{df_j}{dt}$) is governed by the Lotka–Volterra equation:

$$\frac{df_j}{dt} = \frac{\lambda_j \, NPP_j \, f_j}{Cv_j}\left[1 - \sum_j c_{ij}f_j\right] - \gamma_j f_j, \tag{16}$$

where f_j is the fractional coverage of the jth PFT, $\lambda_j \, NPP_j$ is the carbon available for spreading, Cv_j is the carbon density (g C km^{-2}), c_{ij} is the competition coefficient between the ith and jth PFTs, and γ_j (s^{-1}) is the constant disturbance representing the loss of PFT fraction due to fires, pests, windthrow, and many other processes.

When fire model is coupled to SSiB4/TRIFFID, the loss of PFT fraction due to fires (β_j) can be explicitly derived from the fire-induced carbon loss:

$$\beta_j = \frac{(\varphi_j + \psi_j)\cdot f_j}{Cv_j}, \tag{17}$$

where φ_j and ψ_j are PFT-dependent carbon loss due to combustion and post-fire mortality, respectively. The fire-caused PFT fraction loss results in bare soil for vegetation spreading decided by the competition strategy in TRIFFID. As such, fire disturbance is explicitly represented which varies in space and time, and the original γ_j is adjusted to γ_j' to exclude fire disturbance (Table 2):

$$\frac{df_j}{dt} = \frac{\lambda_j \cdot NPP_j \cdot f_j}{C_j}\left[1 - \sum_j c_{ij}f_j\right] - (\gamma_j' + \beta_i)f_j. \tag{18}$$

Table 2. The disturbance rate implicitly including fire disturbance (γ_v) and excluding fire disturbance (γ_v').

	BET	NET	BDT	C3 grasses	C4 plants	Shrubs	Tundra
γ_v	0.004 (0.04 with grasses)	0.004(0.04 with grasses)	0.004 (0.04 with grasses)	0.1	0.1	0.05	0.05
γ_v'	0.004	0.004	0.004	0.02	0.02	0.04	0.01

2.3 Implementing fire model in SSiB4/TRIFFID

In SSiB4/TRIFFID, SSiB4 provides GPP, autotrophic respiration, and other physical variables such as canopy temperature and soil moisture every 3 hours for TRIFFID (Fig. 1). TRIFFID accumulates the 3-hourly GPP and respiration and provides biotic carbon, PFT fractional coverage, vegetation height, and LAI every 10 days, which are used to update surface properties (albedo, canopy height, roughness length, and aerodynamic/canopy resistances) in SSiB4. When the fire model is included, it uses the meteorological forcings and physical variables provided by SSiB4 every 3 hours and the biophysical properties (PFT fraction and biotic carbon) provided by TRIFFID every 10 days. The fire model calculates the burned area, carbon combustion, post-fire mortality, and emissions every 3 hours, and the fire-induced carbon loss is subtracted from fuel load. The carbon loss is accumulated within 10 days in the fire model and is transferred to TRIFFID on Day 10. TRIFFID updates the vegetation dynamics based on carbon balance on Day 10, using the net primary production, fire-induced carbon loss, and PFT competition strategy. The updated vegetation dynamics are transferred to SSiB4 to reflect fire effects on surface properties.

* Red color: inputs for fire model; Green color: inputs for TRIFFID; Blue color: inputs for both Fire and TRIFFID
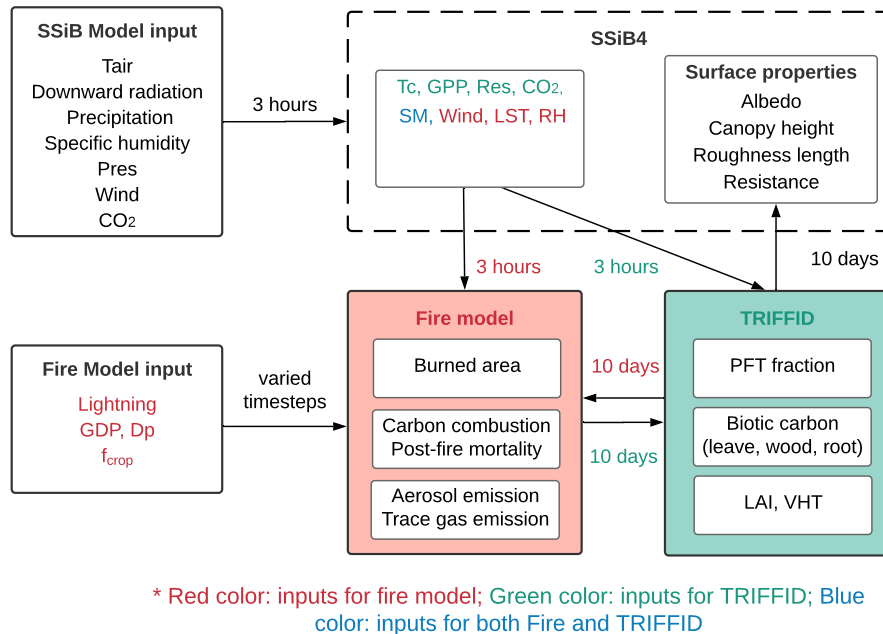
Figure 1. Schematic diagram of fire model coupling in SSiB4/TRIFFID-Fire (Tair: air temperature; Pres: surface pressure; Dp: population density; f_{crop}: crop fraction; Tc: canopy temperature; Res: autotrophic respiration; SM: soil moisture; LST: land surface temperature; RH: relative humidity; VHT: vegetation height)

3. Experimental setup and data

3.1 Experimental design

Two sets of offline experiments have been conducted using SSiB4/TRIFFID-Fire, which consist of FIRE-ON (SSiB4/TRIFFID-Fire with fire model switched on) and FIRE-OFF (SSiB4/TRIFFID-Fire with fire model switched off). To obtain the initial conditions for these two experiments, similar to our previous SSiB4/TRIFFID experiments (Zhang et al., 2015; Liu et al., 2019), we conducted spin-up simulations ($SP_{FIRE-ON}$ and $SP_{FIRE-OFF}$) for 100 years to reach a quasi-equilibrium PFT distribution with and without fire disturbance. These spin-up simulations were initialized using the quasi-equilibrium state from Liu et al. (2019, SP_{INIT} in Fig. 2) and were driven by climatology forcing averaged in 1948-1972 and atmospheric CO_2 concentration, population density, and GDP in 1948 (Fig. 2). Following Liu et al. (2019), the quasi-equilibrium status is

defined as the rate of relative change in fractional coverage of all PFTs is less than 2 % over the last 10 years of simulation.

285   Based on the quasi-equilibrium status with fire disturbance ($SP_{FIRE-ON}$), a transient run was performed (FIRE-ON) with the fire model turned on from 1948 to 2014 (Fig. 2). The model was forced by 3-hourly meteorological forcings, yearly updated atmospheric CO_2 concentration, population density, and GDP data. FIRE-ON produced the fire regime, ecosystem, and surface conditions during 1948-2014. A FIRE-OFF run, based on $SP_{FIRE-OFF}$, was carried out with the fire model switched off during 1948-2014. The vegetation distribution was allowed to respond to climate variations in both FIRE-ON and FIRE-OFF simulations and to fire disturbances only in the FIRE-ON.
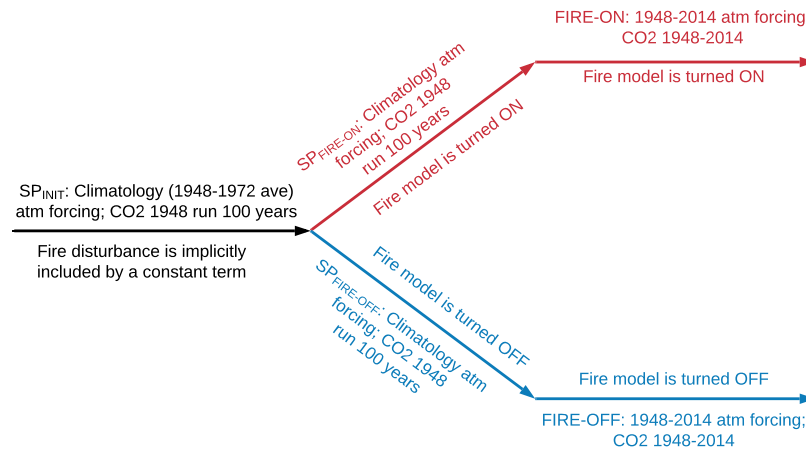
Figure 2. Experiment design for FIRE-ON and FIRE-OFF experiments

295   **3.2 Model input and validation data**

The meteorological forcings used to drive SSiB4/TRIFFID-Fire for the period of 1948–2014 are from the Princeton global meteorological dataset for land surface modeling (Sheffield et al., 2006), including surface air temperature, surface pressure, specific humidity, wind speed, downward shortwave radiation flux, downward longwave radiation flux, and precipitation (Table

300 3). The dataset is constructed by combining global observation-based datasets with the

NCEP/NCAR reanalysis. The spatial resolution is 1.0°×1.0°, and the temporal interval is 3 hours.

The required inputs for driving the fire model are listed in Table 3. The 2-hourly

climatology lightning flashes data from NASA LIS/OTD v2.2 at 2.5°×2.5° resolution is used to

calculate the number of natural ignitions. The population density data are provided by the Gridded

305 Population of the World version 3 (GPWv3; CIESIN, 2014) for 1990-2005 and Database of the

Global Environment version 3.1 (HYDEv3.1; Goldewijk et al., 2010) for 1850−1980. GDP per

capita in 2000 is from van Vuuren et al. (2007). The population density and GDP data are used to

calculate the human ignitions and suppression in the fire model. The agriculture fraction is

obtained from the GLC2000, which represents the agriculture distribution for the year 2000

310 (Bartholome and Belward, 2005). All the datasets are resampled to 1.0°×1.0° spatial and 3-hourly

temporal resolution.

Table 3. Datasets used to drive SSIB4/TRIFFID-Fire and evaluate simulations

Variables	Sources	Resolution
Surface air temperature Surface pressure Specific humidity Wind speed Downward shortwave radiation Downward longwave radiation Precipitation	Sheffield et al. (2006)	1°, 3-hourly
Lightning frequency	NASA LIS/OTD v2.2	2.5°, 2-hourly
Population density	GPWv3 (CIESIN, 2005); HYDE v3.1 (Klein Goldewijk et al., 2010)	0.5°, 5 yearly 5', 10 yearly
Gross domestic product (GDP)	van Vuuren et al. (2006)	0.5°, in 2000
Agriculture fraction Vegetation distribution	GLC2000 (Bartholome et al., 2002)	1°, in 2000
Burned area Carbon emission	GFED4s (Randerson et al., 2012; van der Werf et al. 2017)	0.25°, monthly
CO emission	Zheng et al. (2019)	3.75° lon ×1.9° lat, monthly

| GPP | FLUXNET-MTE (Jung et al. 2009) | 0.5°, monthly |

The Global Fire Emission Database (GFED) is a fire dataset derived mainly from MODIS

315   satellite observations (van der Werf et al., 2006; van der Werf et al., 2010; Giglio et al., 2013).

The GFED fire product provides the burned area and fire emissions on the global scale and has

been widely used for fire model validation and calibration (van Marle et al., 2017; Li et al., 2019).

The latest version of GFED, GFED4s, has included the contribution from small fires that are below

the MODIS detection limit (van der Werf et al., 2017). The burned area and carbon emissions

320   simulated by SSiB4/TRIFFID-Fire will be validated using gridded monthly GFED4s fire products

in 2000–2014 at 0.25° spatial resolution.

We also evaluate the simulated vegetation distribution, CO emission from fire, and GPP

with observations. We use the vegetation fraction from GLC2000 generated in Liu et al. (2019) by

calculating the percentage of each land cover type in 1.0°×1.0° and converting to PFTs in

325   SSiB4/TRIFFID-Fire. The CO emission from Zheng et al. (2019) is an inversion-based product

that uses CO emission from multiple sources as prior, and performs inversion simulations

constrained by atmosphere CO concentration retrieved from the satellite. It provides the latest CO

emission estimate from fire in 2000-2017. FLUXNET Model Tree Ensemble (FLUXNET-MTE)

GPP is upscaled from FLUXNET observations to the global scale using the machine learning

330   technique MTE (Jung et al., 2011). The FLUXNET-MTE GPP at 0.5°×0.5° spatial resolution in

1982–2011 has been resampled to 1.0°×1.0° to be compared with SSiB4/TRIFFID-Fire.

4. Results

This section evaluates the model simulation of burned area, carbon emissions, PFT

fraction, and GPP by comparing FIRE-ON results with GFED4s, GLC2000, and FLUXNET-MTE

335   data. Specifically, we will focus on the model description of fire seasonality. After model

validation, SSiB4/TRIFFID-Fire is applied to assess the long-term fire effect on the ecosystem and surface energy budget using the differences between the FIRE-ON and FIRE-OFF.

4.1 Burned Area

The simulations of burned area are evaluated using satellite-based product GFED4s for the period of 2000-2014. Figure 3 shows the 2000-2014 annual burned fraction in GFED4s and SSiB4/TRIFFID-Fire and their latitudinal distribution. The simulated global burned area is 471.9 Mha yr^{-1}, slightly higher than the estimate from MODIS Collection 6 in 2002-2016 (423 Mha yr^{-1}; Giglio et al., 2018) but very close to the value from GFED4s (478.1 Mha yr^{-1}). The spatial distribution of observed burned area is well captured in the SSiB4/TRIFFID-Fire simulation with a spatial correlation of 0.80. Both GFED4s and SSiB4/TRIFFID-FIRE show that the major burned area is concentrated in the tropical savannas (5-15º N; 5-20º S), including the Northern Hemisphere African (NHAF), Southern Hemisphere African (SHAF), Southern Hemisphere South American (SHSA), and northern Australia (Figs. 3a and 3c). GFED4s shows that the Northern African savanna has a larger latitudinal burned area in a narrower fire band compared to the Southern African savanna (Fig. 3b). SSiB4/TRIFFID-Fire captures the latitudinal band in burned Northern African savanna but underestimates its magnitude (Fig. 3d). Another burned area peak occurs around 50º N in Boreal Asia (BOAS) and Boreal North America (BONA). The humid climate there suppresses fire ignition yet the high level of aboveground biomass and a lack of human suppression facilitate fire occurrence and spread, which results in an intermediate burned area in the boreal regions. The low burned fraction for deserts and tropical rainforests, which is caused respectively by low fuel availability and combustibility, are also well simulated (Fig. 3a), leading to the minimum burned area around the equator and subtropical regions.
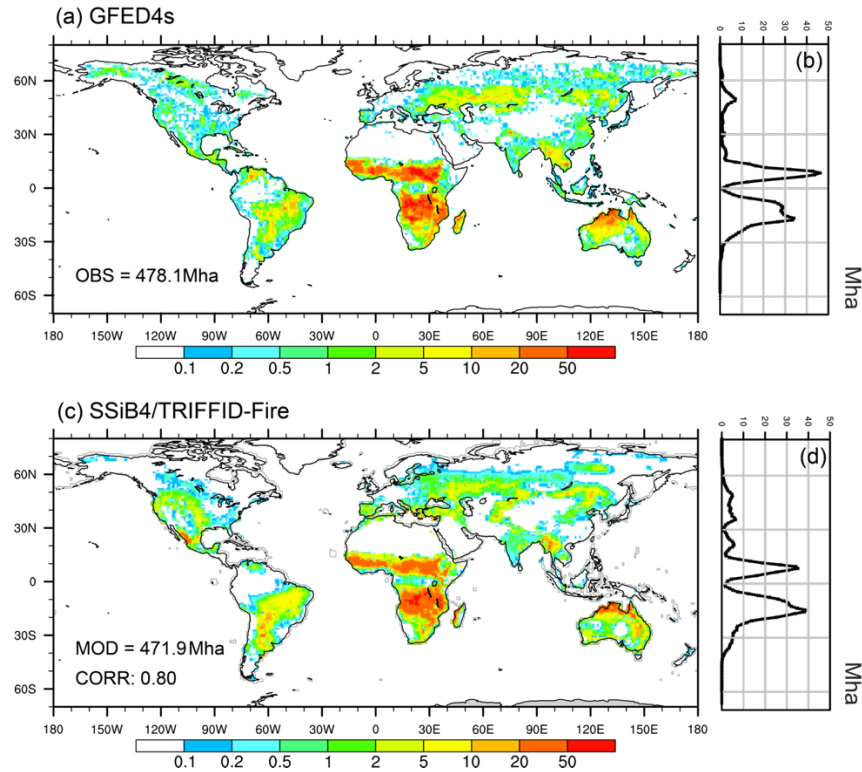
Figure 3. Spatial distribution of annual burned fraction (%) averaged over 2000–2014 for (a) GFED4s and (c) SSiB4/TRIFFID-Fire. The right panel shows the zonal mean burned area (Mha) for (b) GFED4s and (d) SSiB4/TRIFFID-Fire

We also evaluate the 14 sub-regions following the definition in GFED according to the fire behavior similarity (van der Werf et al., 2006). The burned area in African savanna accounts for more than 60 % of the global burned area in both GFED4s and SSiB4/TRIFFID-Fire (Fig. 4b). The simulated burned areas in SHAF and NHAF are 168.3 Mha and 124.5 Mha, respectively, very close to GFED4s burned areas in SHAF (167.9 Mha) but slightly underestimated in NHAF (155.5 Mha). The negative bias in NHAF burned area is the main cause of the underestimation in the latitudinal fire distribution around 10° N (Fig. 3d). SSiB4/TRIFFID-Fire also captures the burned fraction in other major fire regions such as Australia (AUST) and SHSA (Fig. 4b), which are dominated by savanna fire. We notice that the burned area in western and central parts of temperate North America (TENA) is overestimated (Figs. 3c and 4b). Nevertheless, the burned area there is

relatively small compared to that in major fire regions such as SHAF and NHAF. This shortcoming has been reported in a number of fire models (Pfeiffer and Kaplan, 2012; Lasslop et al., 2014; Yue et al., 2014; Venevsky et al., 2019). The reasons include an underestimate of anthropogenic suppression, inaccurate description of fuel pattern/grassland fraction, and landscape fragmentation from roads and other anthropogenic features. The burned area in the Middle East (MIDE) is also overestimated (Fig. 4b) as a larger burned area is simulated at the northern boundary of the Sahara Desert and south of the Black Sea (Fig. 3c). The simulated burned area is underestimated in BONA and BOAS where fire has a lower incidence but a longer duration compared to the global average (Ward et al., 2018; Venevsky et al., 2019). As we assume all fires persist for one day, the burned area in boreal regions is therefore underestimated. Further improvements, such as multi-day burning and a deliberate scheme for anthropogenic effect, are necessary in regional applications.

In 8 out of the 14 sub-regions, SSiB4/TRIFFID-Fire well reproduces the observed interannual variability (IAV) of burned area, with the correlation between simulations and observations significant at $p < 0.05$ (Fig. 4c). The regions are NHAF, SHSA, AUST, TENA, Central America (CEAM), Europe (EURO), Southeast Asia (SEAS), and Equatorial Asia (EQAS). In particular, a decline in NHAF burned area is found in both SSiB4/TRIFFID-Fire and GFED4s, which has been attributed to agricultural expansion and intensification in recent fire studies (Andela et al., 2017; Teckentrup et al., 2019). Although our model does not have an explicit description of agriculture fraction and intensification changes, the anthropogenic effect is implicitly included by relating fire suppression to population density and GDP (Li et al., 2013). Meanwhile, SSiB4/TRIFFID-Fire also captures the IAV in SEAS and EQAS, which is known to be driven by climate factors such as relative humidity and soil moisture.
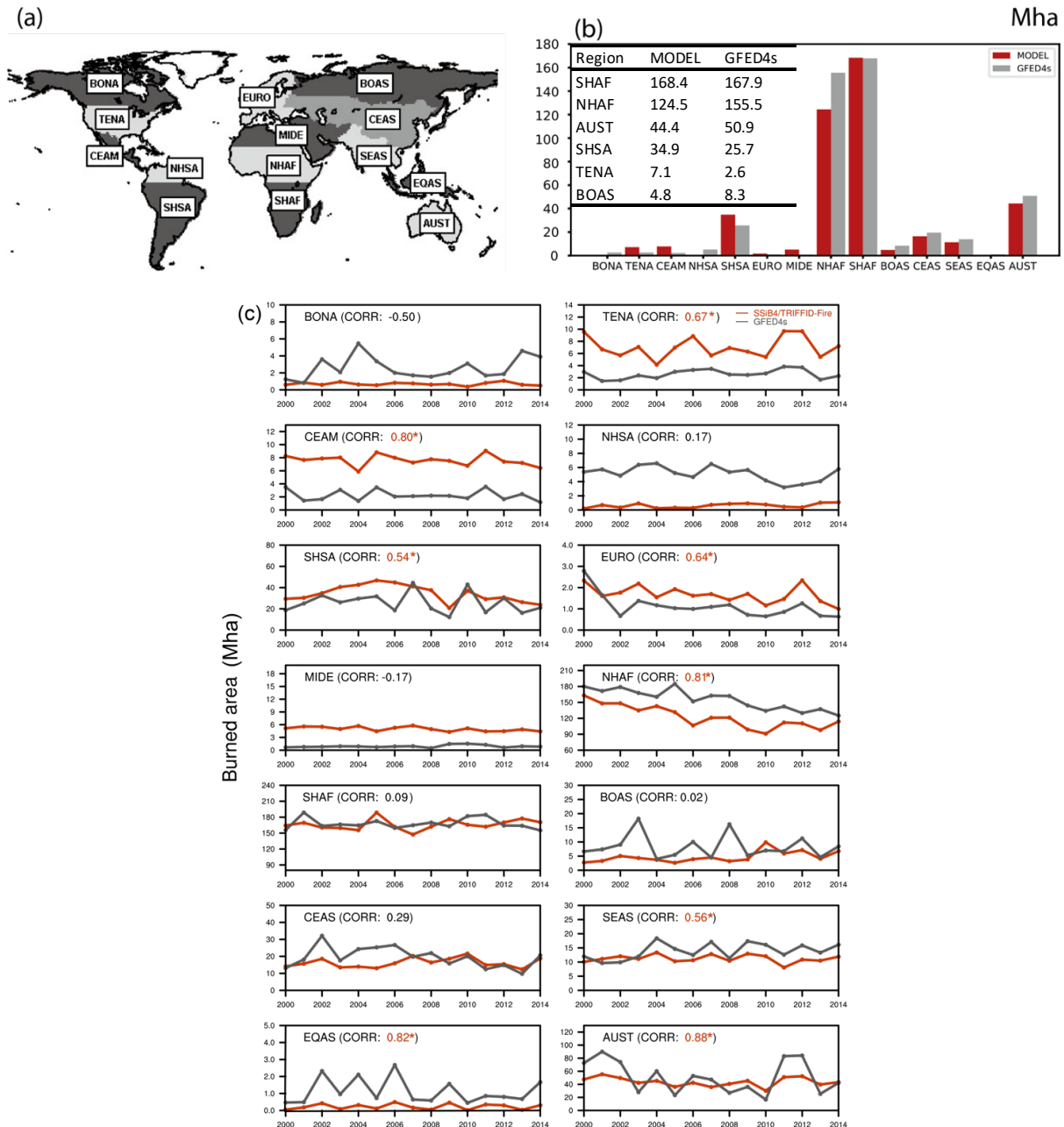
Figure 4. (a) Map of 14 regions used in this study, after Giglio et al. (2006, 2010) and van der Werf et al. (2006, 2010) (b) Annual burned area (Mha) averaged over 2000-2014 for GFED4s and SSiB4/TRIFFID-Fire in 14 regions (c) Annual burned area (Mha) for 2000–2014 for GFED4s and SSiB4/TRIFFID-Fire in 14 GFED regions. The "*" and the red color indicate the positive correlation is significant at $p < 0.05$.

The simulated IAV of SHAF burned area is not as good as other savanna fire regions (e.g., NHAF, SHSA, and AUST), although the IAV is small there (Fig. 4c). Some studies have reported

that humans have a substantial impact on SHAF fire, which limits the effect of climate-induced

IAV (Archibald et al., 2010; Venevsky et al., 2019). In addition, the simulated IAV of burned areas

405   is lower than observations in BONA and BOAS as the model fails to capture some extreme fire

events (Fig. S1). The lower variability comes from the climatology lightning data (Pfeiffer et al.,

2013). As lightning flash is the predominant ignition source in the Northern Hemisphere high

latitudes, the application of climatology lightning has a greater impact in boreal regions than in

other parts of the globe.

410   Figure 5 shows the pointwise temporal correlation of the multi-year monthly burned area

between SSiB4/TRIFFID-Fire and GFED4s averaged in 2000-2014. SSiB4/TRIFFID-Fire

captures the fire seasonality in most regions, including the Southern African savanna, South

American savanna, the northeastern part of Boreal Asia, the eastern part of Boreal America,

Southeast Asia, and Equatorial Asia. Specifically, we examine the simulation of peak fire month

415   and fire season length in SSiB4/TRIFFID-Fire following the definition that fire seasons include

months with more than 1/12 of the mean annual burned fraction (Venevsky et al., 2019). Over the

globe, August and December are the two peak fire months that have the largest contribution to the

annual burned area (Fig. 6a). SSiB4/TRIFFID-Fire generates two fire seasons in June-July-August

and December-January-February, capturing the peak month in August but underestimating the

420   burned area in December. In the tropical savannas (SHAF, SHSA, and NHAF), fire activities

concentrate in the local dry season, and the burned area during the fire season accounts for more

than 80 % of the annual burned area (Figs. 6b-d). The burned area in Southern Hemisphere major

fire regions, SHAF and SHSA, peaks in August and September in both observations and model.

The simulated fire seasons in SHAF (June-October) and SHSA (July-October) match precisely

425   with the observations. In other fire regions such as SEAS and EQAS, SSiB4/TRIFFID-Fire also

reproduces the fire seasonality and peak fire months (Figs. 6e-f). Compared with the latest results from other fire models (Hantson et al., 2020), our model produces more realistic burned area peak and fire season duration.

Figure 5 shows, however, that the fire seasonality in the Northern Hemisphere Africa, the
430 western part of Boreal Asia, eastern China, western Australia, and the middle eastern US needs to be improved. The simulated fire season in West Africa is December-March (Fig. 6d), slightly shifted from the fire season in GFED4s (November-February), which contributes to the lower fire peak in December in the global burned area. The recent FireMIP models also show a 2-months delay in peak fire month in Northern tropics (Hantson et al., 2020), which might be related to the
435 representation of seasonality in vegetation production and fuel build up. In BOAS, the first fire season occurs in April and May. The observed fire season is not captured in SSiB4/TRIFFID-Fire as the model underestimates the burned area in western Siberia due to too wet moisture conditions that come from the high precipitation and specific humidity in the forcing data. A similar scenario is found in Western Australia (Fig. 6h). Meanwhile, the absence of crop fire in SSiB4/TRIFFID-
440 Fire also contributes to the low temporal correlation with the observations in agricultural areas such as the middle eastern US and eastern China, where fires are used to clear the crop residues (Xia et al., 2013; van der Werf et al., 2017).
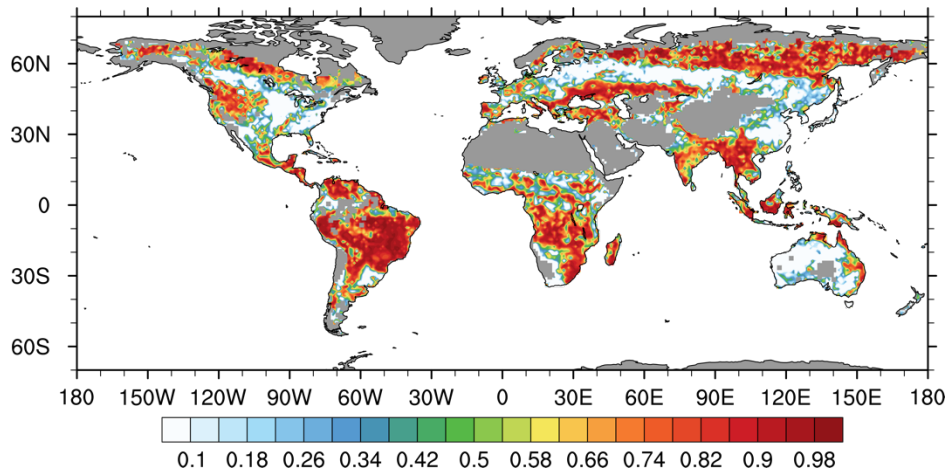
Figure 5. Temporal correlation of monthly burned area averaged over 2000-2014 between SSiB4/TRIFFID-Fire and GFED4s (grids with annual burned fraction < 0.001 % are masked)

Overall, SSiB4/TRIFFID shows good consistency in the simulation of peak fire month and fire season duration in most regions, probably related to the better representation of vegetation-fire interactions in SSiB4/TRIFFID-Fire which updates fire effects on vegetation dynamics every 10 days. The inaccurate simulation of fire season in several fire regions could come from deficiency of the forcing data, the inaccuracy in dynamic vegetation processes, or some processes that control the fire but are not represented in the model. More comprehensive observational data are needed to improve the simulation in these areas.
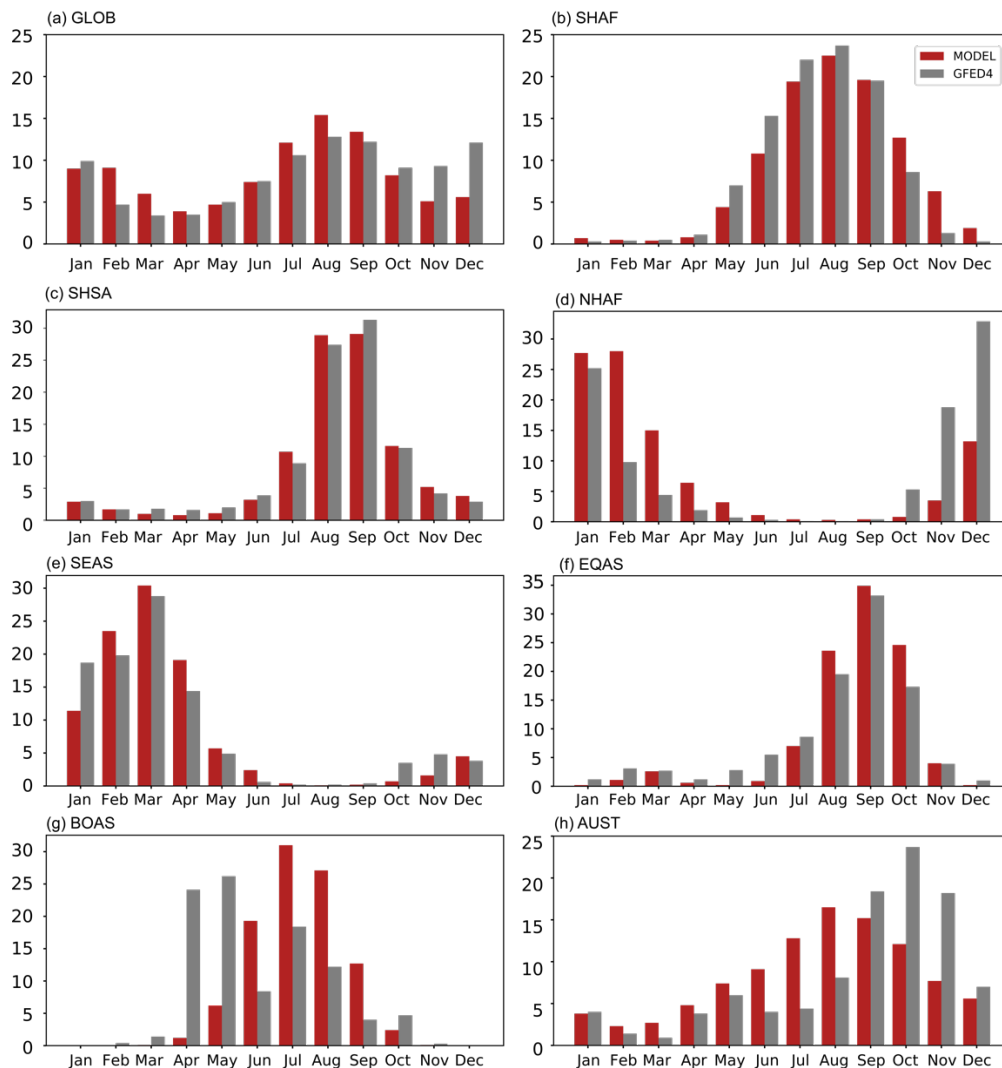
Figure 6. The contribution of monthly burned area to annual burned area (%) over the (a) GLOB, (b) SHAF, (c) SHSA, (d) NHSA, (e) SEAS, (f) EQAS, (g) BOAS, and (h) AUST averaged over 2000-2014 for SSiB4/TRIFFID-Fire and GFED4s

4.2 Fire emissions

Biomass burning emissions are determined by burned area, fuel combustion rate per unit area, and emission factors per unit mass of fuel burned (van der Werf et al., 2017). The carbon emission in SSiB4/TRIFFID-Fire is 2.19 Pg yr^{-1}, higher than the estimate from GFED4s (2.07 Pg yr^{-1}) (Fig. 7). SSiB4/TRIFFID-Fire captures the high carbon emissions in tropical savannas, the intermediate emissions in Northern Hemisphere boreal forests, and the low emissions in humid forests and deserts with a spatial correlation of 0.72, higher than the simulation in Li et al. (2013) (0.61 compared with the GFED3). In general, the spatial distribution of carbon emissions coincides with that of the burned area: SHAF, NHAF, and SHSA are the major fire emission regions and they contribute to 65.4% of the total emission in both GFED4s and SSiB4/TRIFFID-Fire (Fig. 8a). The exception occurs in EQAS, BOAS, and BONA, where the fire emissions contribute to 11.6 % of the global emissions with only 2.5 % of the global burned area there. The regions have large areas of peatland, which contains a thick layer of soil carbon and emits several times more trace gases per unit biomass combusted than fires in savannas (van der Werf et al., 2010). As our model does not include the peat soil type, fire emissions are underestimated in these regions.
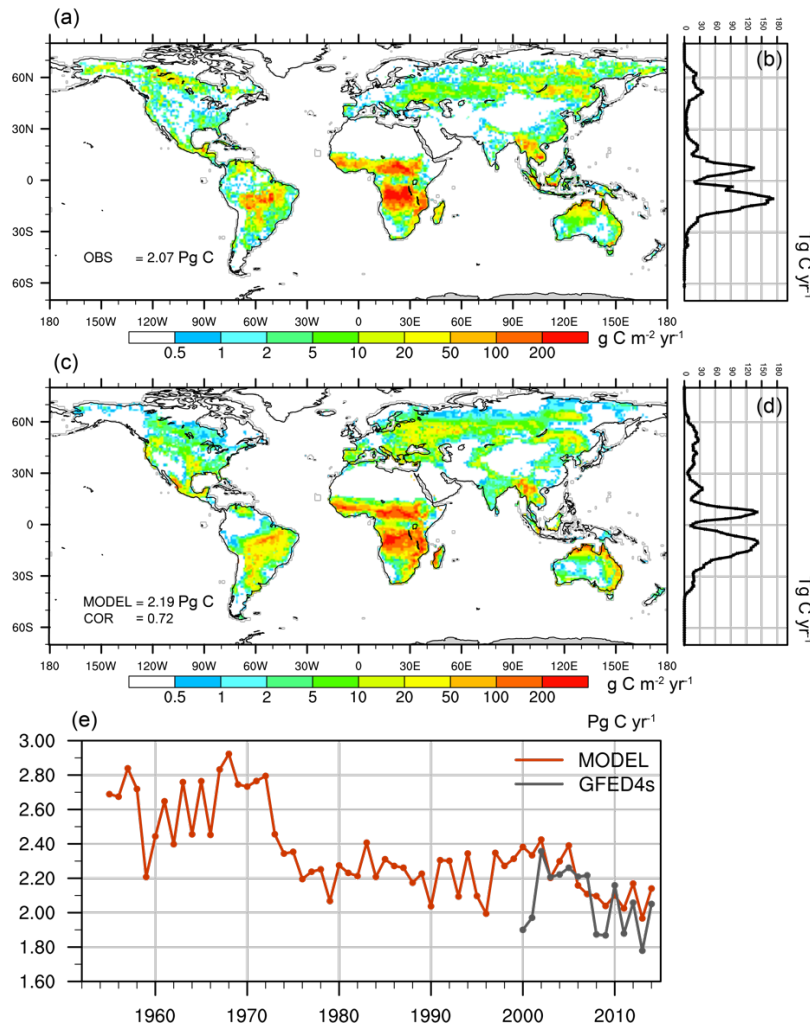
Figure 7. (a) Spatial distribution of annual carbon emission (g C yr^{-1}) averaged over 2000–2014 for GFED4s and (b) the latitudinal distribution of carbon emission (Tg C yr^{-1}); (c), (d) Same as (a), (b) but for SSiB4/TRIFFID-Fire (g C yr^{-1}); (e) Annual carbon emission (Pg C yr^{-1}) for GFED4s for 2000-2014 and for SSiB4/TRIFFID-Fire for 1948-2014

The interannual variability (IAV) of fire emissions is captured in SSiB4/TRIFFID-Fire in 7 out of 14 fire regions with a significance level $p < 0.05$ (Fig. S2). Both model and observations have shown a decrease in carbon emissions in NHAF (Fig. 8b), which contributes to the decrease in global fire emission in 2000-2014 (Fig. 7e). SSiB4/TRFFID-Fire suggests that the decline of global fire emissions starts in the 1950s, which is also found in some of the FireMIP models (Li et al., 2019). Similar to our conclusions in the IAV of burned areas, the IAV of carbon emissions in SHSA is small and is not well represented in the model (Fig. 8c).
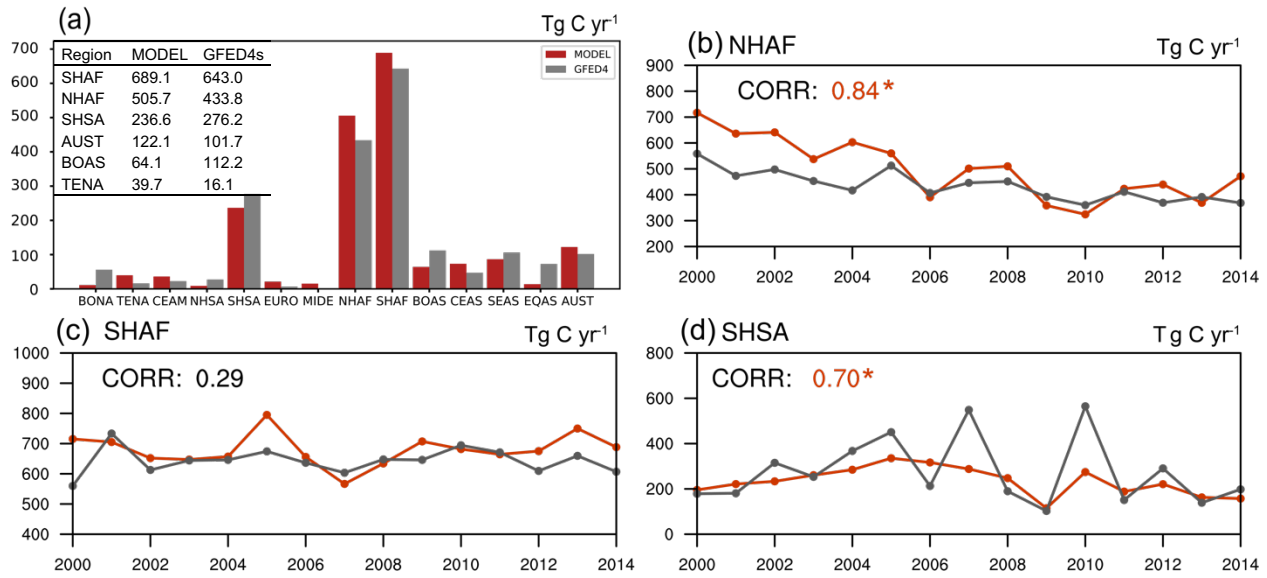
Figure 8. (a) Annual carbon emission averaged over 2000-2014 for GFED4s and SSiB4/TRIFFID-Fire in 14 GFED regions; (b)-(d) annual carbon emission in (b) SHAF, (c) NHAF, and (d) SHSA for 2000–2014 for GFED4s and SSiB4/TRIFFID-Fire. The "*" and red color indicate the correlation is significant at p < 0.05.

The CO emission from fire is one of the key variables in fire modeling as CO plays a vital role in atmospheric chemistry. The simulated global CO emission is 433.7 Tg year^{-1} in 2000-2014, very close to the observational estimates (434.0 Tg year^{-1}) from Zheng et al. (2019) with a spatial correlation of 0.74. The inversion-based and simulated monthly CO emissions in Africa are compared in Fig. 9. We find the annual cycle of CO emission in SHAF is well captured in SSiB4/TRIFFID-Fire, which shows the largest CO emission occur in JJAS and the regions with high-emission (Fig. 9b) are coincident with those in observations (Fig. 9a). In NHAF, SSiB4/TRIFFID-Fire reproduces the large CO emission in DJF, although the model slightly underestimates CO emission in December and overestimates it in February. The seasonality of CO emission broadly follows that of burned area, which further demonstrates that our model has shown promising results in seasonal fire simulations.
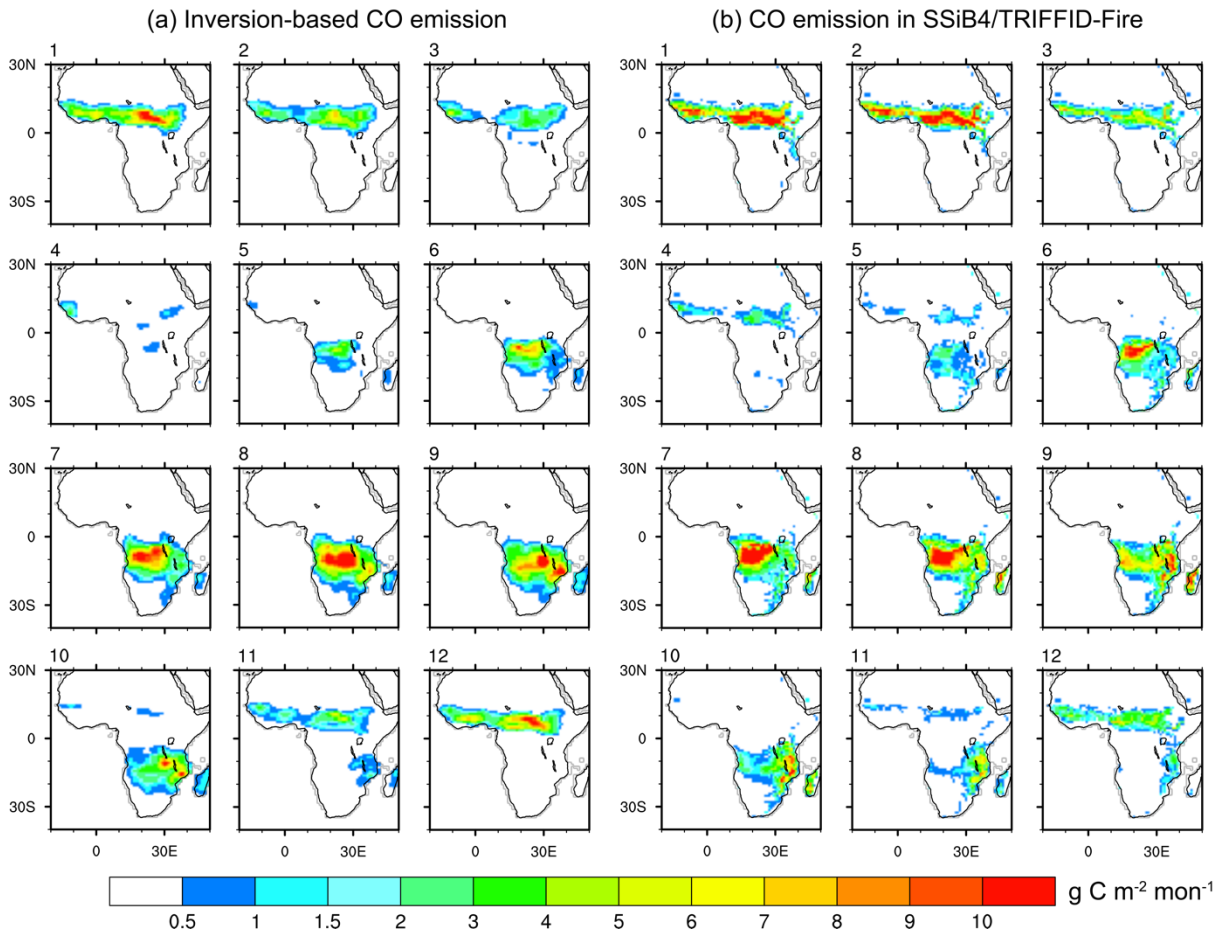
Figure 9. Monthly CO emission in Africa averaged in 2000-2014 from (a) Zheng et al. (2019) and
505   (b) SSiB4/TRIFFID-Fire

4.3 PFT distribution and GPP

The simulation of vegetation coverage, which represents model description of biomass
510   allocation and influences the fuel availability and flammability in fire modeling, is evaluated

against GLC2000 (Bartholome and Belward, 2005). As the dynamic vegetation model only

includes natural PFTs, the simulated PFT fraction in one grid box is scaled using the non-

agriculture fraction from GLC2000. Overall, the vegetated areas cover 80.6 % of global land areas,

very close to the estimates from GLC2000 (80.8 %). The simulated tree cover is 34.1 %, higher

515   than 29.8 % in GLC2000. Compared with the observations (Fig. 10a), SSiB4/TRIFFID-Fire

captures the fractional coverage of trees in the Amazon rainforest, tropical Africa, Equatorial Asia,

Southeast Asia, Southeast North America, and Northern Hemisphere Boreal regions (Fig. 10c). The BET is concentrated in tropics, and the NET is mostly found in the North America and Eurasia Boreal zones (Figs. S3a-c). The C3 and C4 grasses are found in the Northern Hemisphere Africa,

520 Southern Africa, South America, Central US, Eurasian steppes, and east Australia (Figs. 10b and 10d). The simulated C3 and C4 fractions are 11.1 % and 7.5%, respectively, similar to the estimates in GLC2000 (11.9 % for C3 and 7.9 % for C4; Liu et al. 2019). Shrubs are primarily located in the semi-arid regions and the pan-Arctic area and tundra is limited to the pan-Arctic area and Tibetan Plateau (Figs. S3f-g). SSiB4/TRIFFID-Fire is shown to capture some key processes of fire-

525 vegetation interactions under the current climate, which is important to study fire effects on the ecosystem.
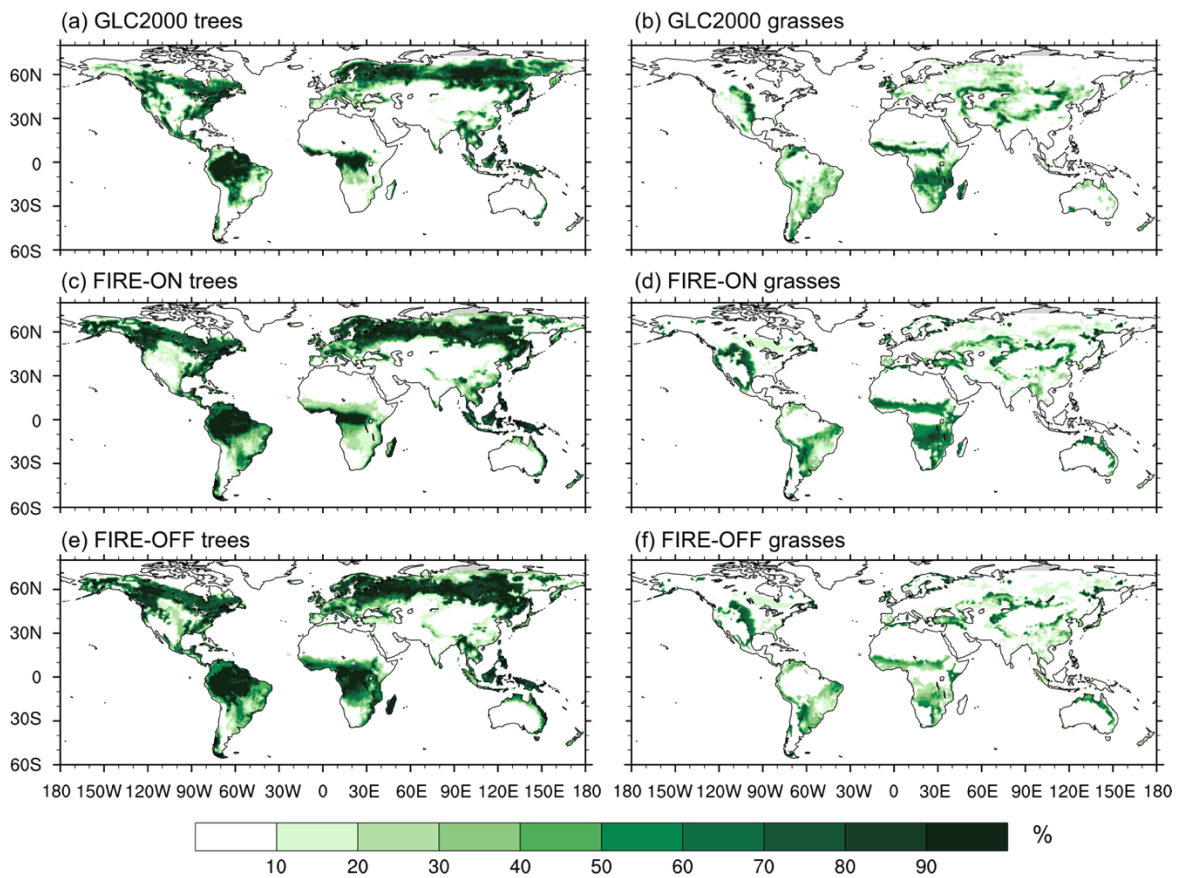
Figure 10. The fractional coverage of trees in (a) GLC2000, (c) FIRE-ON, and (e) FIRE-OFF and the fractional coverage of grasses in (b) GLC2000, (d) FIRE-ON, and (f) FIRE-OFF in 2000

We also compare the simulated GPP averaged over 1982-2011 to FLUXNET-MTE GPP (Jung et al., 2011) to examine the modelled impact of fire on carbon. SSiB4/TRIFFID-Fire captures the distribution of global GPP with a spatial correlation of 0.93 (p < 0.05) (Fig. S4). The highest GPP occurs in the tropical evergreen forest and decreases with latitude in both observations

535   and model. However, the simulated GPP has a negative bias in the Amazon tropical forest and a positive bias in tropical Africa and boreal regions. The simulated global GPP is 141 Pg C yr^{-1}, higher than the FLUXNET-MTE estimate (119 Pg C yr^{-1}; Jung et al., 2011), but is within the range of simulated GPP in current DGVMs (111 - 151 Pg C yr^{-1}; Piao et al., 2013). In addition, the correlation of IAV of global GPP is 0.68 (p < 0.05) between SSiB4/TRIFFID-Fire and FLUXNET-

540   MTE, indicating that the model has reasonably captured the terrestrial ecosystem variability during the historical period.

4.4 Fire effects on ecosystem characteristics and surface properties

In this section, we investigate long-term fire effects on ecosystem characteristics, surface properties, and surface energy budget using the differences between FIRE-ON and FIRE-OFF

545   (FIRE-ON minus FIRE-OFF). In SSiB4/TRIFFID-Fire, fire is found to cause a strong decrease in tree fraction by 12.6 % (about 4.5 % of the land surface). Meanwhile, the fractional coverage of grass and bare land is increased on 3.4 % and 0.5 % of the land surface, respectively (Figs. 11a-b). The tree cover reduction is concentrated in Southern Africa, Northern Africa, and South America, which are dominated by C4 savanna in FIRE-ON (Fig. S3), suggesting that fire is an important

550   determinant of structure and functions of the savanna; otherwise it would be encroached by trees. The magnitude of change simulated is generally consistent with the results from long-term fire experiments in Kruger National Park, South Africa, which showed that fire reduced woody cover by 30-50% (Smit et al., 2010). The changes in the fractional coverage of trees and grass are

associated with tree mortality after fire and the fast re-growth of grass PFTs with space and nutrient

555   availability during the post-fire recovery season. Over the globe, fire is simulated to reduce LAI

by 3.6% (0.10 m^2 m^{-2}) and shorten vegetation height by 12.7% (1.24 m).

In Africa, the simulated fire effects on vegetation structure (tree/grass cover, LAI, and

vegetation height) peak in the tropical savanna surrounding the forests and gradually decrease

towards the deserts (Fig. 11). When fire model is turned off, the tree cover expands in the wetter

560   savanna around the tropical African forest where the climate (mainly rainfall in the model) allows

for more trees to approach canopy closure such that grasses can be effectively excluded (Fig. 10e).

The grass cover shrinks to the southern/northern part of Southern/Northern African savanna (Fig.

10f), where tree populations are constrained by environmental conditions.

Our results are consistent with the long-term fire experiments which reported that fire

565   strongly affected vegetation structure, lowering the proportions of trees to fire-resistant grasses

and reducing the vegetation height and aboveground biomass (Shackleton and Scholes, 2000;

Higgins et al., 2007; van Wilgen et al., 2007; Furley et al., 2008; Smit et al., 2010; Devine et al.,

2015), and that fire impact is more remarked in wetter savanna than in drier savanna (Moreira,

2000; Sankaran et al., 2005). However, the long-term fire experiments were only conducted in

570   very limited regions and mostly focused on site-level fire impact (Furley et al., 2008). The

assessment of continental and global fire impact on vegetation and carbon can only be achieved

by fire-coupled DGVMs. After appropriate validation of fire effects on the local scale,

SSiB4/TRIFFID-Fire can be used as an effective tool to describe the climate potential of the

ecosystem without fire disturbance and to quantify fire impact on the global scale.
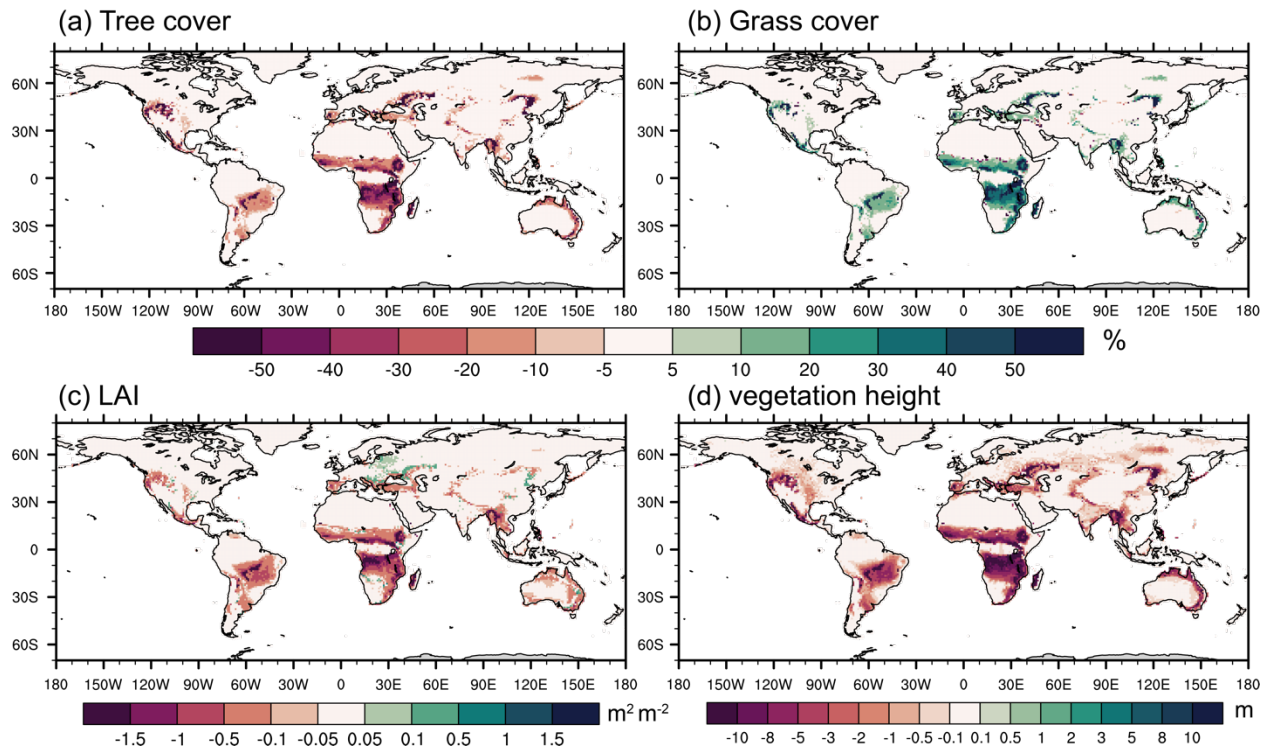
Figure 11. Differences in (a) tree cover (BET, NET, and BDT; %) (b) grass cover (C3 and C4; %), (c) LAI (m^2 m^{-2}), and (d) Vegetation height (m) in SSiB4/TRIFFID-Fire averaged over 2000-2014 between FIRE-ON and FIRE-OFF

The changes in vegetation structure modify the albedo, aerodynamic resistance, and evapotranspiration processes, which further influences surface radiation and energy partitioning between latent heat and sensible heat fluxes. In this study, we investigate seasonal fire impact by distinguishing between fire season (DJF for NHAF, and JJA for SHAF and SHSA) and post-fire rainy season (JJA for NHAF, and DJF for SHAF and SHSA) for major fire regions. Because grass PFTs have a higher albedo than tree PFTs, the replacement of trees by grasses/savannas (Figs. 11a-b) has caused an increase in grid-average albedo, which decreases the net radiation absorbed by surface (Figs. 12a-b). The reduction in surface radiation is larger in fire season (DJF for NHAF, and JJA for SHAF and SHSA) as the exposure of bare land after fire further enhance the albedo. The reduction in vegetation height between FIRE-ON and FIRE-OFF (Fig. 11d) has significantly decreased the roughness length and increased the aerodynamic resistance (Liu et al., 2016), which

590 causes a reduction of sensible heat flux by 4-8 W m^{-2} (Figs. 12c-d). Our results are in agreement with the observational studies on different fire types (e.g., forest fire and savanna fire) showing that surface properties change after fire results in an increase in albedo (Gholz and Clark, 2002; Amiro et al., 2006b; Sun et al., 2010) and a decrease in sensible heat (Chambers and Chapin, 2002; Liu et al., 2005; Amiro et al., 2006a; Amiro et al., 2006b; Rogers et al., 2013).

595 The change of latent heat flux varies with seasons in tropical savanna. It is reduced in the fire season and enhanced in the rainy season for each fire region (Figs. 12 e-f). In SSiB4, the grid-average latent heat flux consists of canopy evapotranspiration, canopy interception, and soil evaporation, among which canopy interception normally plays a minor role. During the local fire season, the canopy transpiration is decreased (Fig S5a-b) due to fire-induced vegetation canopy

600 loss. The soil evaporation does not change too much as there is not much surface water to evaporate (Fig S5c-d). Therefore, the grid average latent heat is decreased. During the post-fire rainy season, the canopy transpiration is still reduced as the vegetation has not recovered from the fire. However, the exposure of bare soil has produced more soil evaporation. Therefore, the latent heat can be increased due to enhanced soil evaporation. The significant increase in soil evaporation and latent

605 heat during wet season has been widely observed after vegetation removal, especially when the soil is saturated (Langford, 1976; Dunin, 1987; Gholz and Clark, 2002; Santos et al., 2003; Amiro et al., 2006b). The increase is proposed to be caused by the exposure of moist soil surface, the increase in surface energy that can be used for evaporation, and the smaller surface resistance when dense plant canopy is removed by fire (Schulze et al., 1994). Despite the reduction in surface

610 radiation, the decreased surface fluxes associated with aerodynamic/surface resistance changes have resulted in an increase in surface temperature throughout the year (Figs. 12g-h).
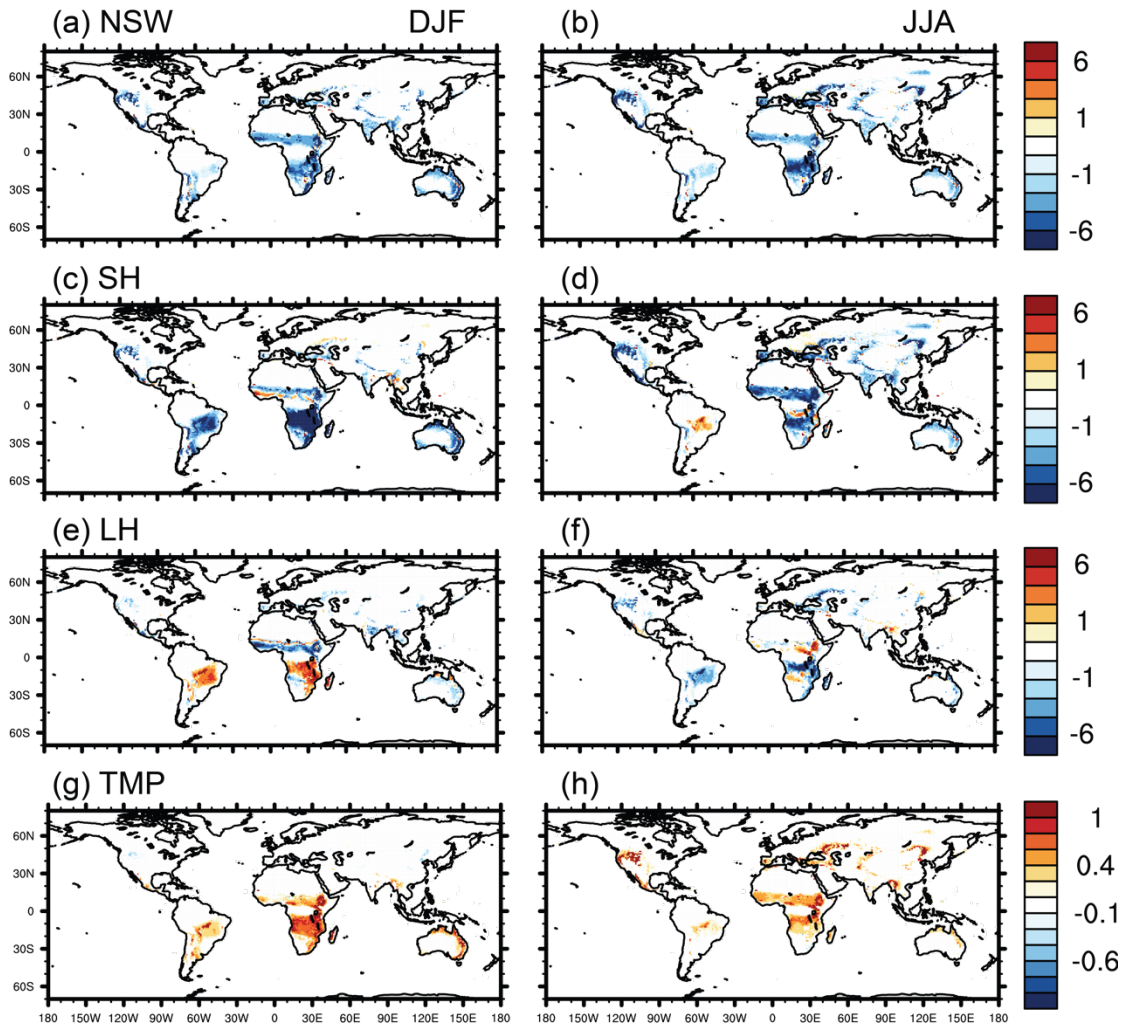
Figure 12. Differences in net shortwave (a, b; W m^{-2}), sensible heat (c, d; W m^{-2}), latent heat (e,f; W m^{-2}), and surface temperature (g, h; K) in DJF (a, c, e, and g), and JJA (b, d, f, and h) averaged over 2000-2014 between FIRE-ON and FIRE-OFF.

Our estimate of fire effects on radiation, surface fluxes, and temperature are qualitatively consistent with Li et al. (2017) but different in the partitioning between sensible heat and latent heat changes. The discrepancies might be attributed to the changes in vegetation distribution. As the vegetation distribution is prescribed in Li et al. (2017), trees and grass are growing taller and denser when the fire model is turned off. In contrast, fire has caused changes in vegetation distribution and conversions of dominant PFTs in SSiB4/TRIFFID-Fire. Tree PFTs are spreading in FIRE-OFF and encroaching the tropical savanna and grassland in Southern Africa, Northern

Africa, and South America shown in FIRE-ON. Over the Africa and South American savanna, we find fire has reduced the area-averaged LAI and vegetation height by 0.52 m^2 m^{-2} (12.5 %) and

625   5.76 m (49.1%), respectively. The larger relative change in vegetation height is simulated as tree PFTs have a greater contrast with grass PFTs in vegetation height than in LAI. Compared with Li et al. (2017), SSiB4/TRIFFID-Fire simulates a greater change in vegetation height but a smaller change in LAI, which probably causes the larger sensible heat changes in our results. Other sources of uncertainties include the differences in the partitioning between latent heat and sensible heat

630   fluxes in land surface models, the differences in the parameterization of the evaporation processes, and the changes due to atmospheric feedbacks, such as cloud cover and precipitation changes.

5. Conclusions and discussions

We have implemented a process-based fire model of intermediate complexity into a DGVM, SSiB4/TRIFFID, which is based on the surface water, carbon, and energy balances, as

635   wells as the PFT competition. The high-frequency exchanges between fire model and SSiB4/TRIFFID allow vegetation dynamics and surface parameters, such as albedo and surface roughness length, to be updated every 10 days based on surface carbon balance, which are rarely applied in other fire models. Moreover, the plant production and biomass allocation are reasonably reproduced in SSiB4/TRIFFID-Fire, which have been considered to contribute to the proper

640   burned area simulation (Forkel et al., 2019; Hantson et al., 2020). The SSiB4/TRIFFID-Fire produces similar global burned area, major regional burned areas, and fire carbon emissions compared to GFED4s. The model captures the decreasing trend in burned area related to human suppression and land management and the interannual variability associated with moisture conditions. It reasonably reproduces the global GPP and PFT distribution, which is important to

645   study fire effects on the ecosystem.

Future development of SSiB4/TRIFFID-Fire are in three aspects. First, SSiB4/TRIFFID-Fire does not explicitly represent the occurrence of peat fire, deforestation fire, and agriculture fire. The inclusion of peat fire and deforestation fire may reduce the negative bias in the burned area and carbon emission in EQAS, BOAS, and BONA, and the parameterization of agriculture fire may improve the fire seasonality simulation in the middle eastern US and eastern China. Second, the effect of agriculture expansion on fire suppression is not considered in current SSiB4/TRIFFID-Fire as we apply a constant agricultural fraction, which is expected to influence the spatial and temporal variations of burned area beyond GDP and population effects (Andela et al., 2017). Third, the carbon cycle in the current SSiB4/TRIFFID version does not explicitly represent the litter carbon storage and decomposition. Therefore, we assume aboveground litter to be 25% and 30% of aboveground biomass for global forest and savanna based on observations from Pan et al. (2011) and de Oliveira et al. (2019). The next generation of SSiB couples SSiB/TRIFFID with DayCent-SOM, which describes the full processes of litter accumulation and decomposition constrained by nitrogen availability (Parton et al., 1994). An explicit scheme for litter combustion will be updated in the fire model in the new SSiB/TRIFFID.

The SSiB4/TRIFFID-Fire is then applied to study the long-term fire effects on ecosystem characteristics and surface energy. By comparing the simulations with and without fire, we show that fire has reduced global tree cover by 12.6 % (4.5 % of land surface). Meanwhile, the global LAI and vegetation height are decreased by 0.10 m^2 m^{-2} and 1.24 m, respectively. The surface radiation, sensible heat, and canopy evapotranspiration are decreased while the soil evaporation is increased especially during the post-fire rainy season. The change in surface fluxes has caused an increase in surface temperature over most fire regions. As Li et al. (2017) is the only modeling study investigating the long-term fire effects on land energy budget, our simulation provides

another approach that quantifies fire effects using a different land surface model with different

670 approaches in parameterizing some land surface processes and vegetation dynamics. More studies

with more land surface models/fire models/vegetation dynamics are necessary to explore this issue

further. A systematic comparison of long-term fire effects in different fire models such as the

current FireMIP project, would allow evaluation of the robustness of model simulations and

identification of key uncertainties of fire impacts.

675

Code availability: The source code of fire model is archived https://zenodo.org/record/3872633#.XtXeeJ70lhE (DOI: 10.5281/zenodo.3872633)

Author contributions: HH, YX, and YL designed the coupling strategy between SSiB4/TRIFFID

680 and fire model. HH conducted the simulation under the suggestions from FL and YL. HH drafted

the text and made the figures. All authors (HH, YX, FL, and YL) have contributed to the analysis

methods and to the text.

Competing interests: The authors declare that they have no conflict of interest.

685

Acknowledgments: This work is supported by NSF Grant AGS-1419526 and AGS-1849654. The

authors acknowledge Cheyenne (doi:10.5065/D6RX99HX) provided by NCAR CISL, for

providing HPC resources. FL acknowledges support from the National Key R&D Program of

China (2017YFA0604302 and 2017YFA0604804).

690

References:

Amiro, B. D., Barr, A. G., Black, T. A., Iwashita, H., Kljun, N., McCaughey, J. H., Morgenstern, K., Murayama, S., Nesic, Z., Orchansky, A. L., and Saigusa, N.: Carbon, energy and water fluxes at mature and disturbed forest sites, Saskatchewan, Canada, Agr Forest Meteorol, 695   136, 237-251, 2006a.

Amiro, B. D., Orchansky, A. L., Barr, A. G., Black, T. A., Chambers, S. D., Chapin, F. S., Gouldenf, M. L., Litvakg, M., Liu, H. P., McCaughey, J. H., McMillan, A., and Randerson, J. T.: The effect of post-fire stand age on the boreal forest energy balance, Agr Forest Meteorol, 140, 41-50, 10.1016/j.agrformet.2006.02.014, 2006b.

700 Andela, N., Morton, D. C., Giglio, L., Chen, Y., van der Werf, G. R., Kasibhatla, P. S., DeFries, R. S., Collatz, G. J., Hantson, S., Kloster, S., Bachelet, D., Forrest, M., Lasslop, G., Li, F., Mangeon, S., Melton, J. R., Yue, C., and Randerson, J. T.: A human-driven decline in global burned area, Science, 356, 1356-1361, 10.1126/science.aal4108, 2017.

Andreae, M. O.: Emission of trace gases and aerosols from biomass burning – an updated 705   assessment, Atmos. Chem. Phys., 19, 8523-8546, 10.5194/acp-19-8523-2019, 2019.

Archibald, S., Nickless, A., Govender, N., Scholes, R. J., and Lehsten, V.: Climate and the inter-annual variability of fire in southern Africa: a meta-analysis using long-term field data and satellite-derived burnt area data, Global Ecol Biogeogr, 19, 794-809, 10.1111/j.1466-8238.2010.00568.x, 2010.

710 Arora, V. K., and Boer, G. J.: Fire as an interactive component of dynamic vegetation models, J Geophys Res-Biogeo, 110, 10.1029/2005jg000042, 2005.

Bachelet, D., Ferschweiler, K., Sheehan, T. J., Sleeter, B. M., and Zhu, Z. L.: Projected carbon stocks in the conterminous USA with land use and variable fire regimes, Global Change Biol, 21, 4548-4560, 10.1111/gcb.13048, 2015.

715 Bartholome, E., and Belward, A. S.: GLC2000: a new approach to global land cover mapping from Earth observation data, Int J Remote Sens, 26, 1959-1977, 2005.

Bistinas, I., Harrison, S., Prentice, I., and Pereira, J.: Causal relationships vs. emergent patterns in the global controls of fire frequency, Biogeosciences, 11, 5087-5101, 2014.

Bond, W. J., Woodward, F. I., and Midgley, G. F.: The global distribution of ecosystems in a world 720   without fire, New Phytol, 165, 525-537, 10.1111/j.1469-8137.2004.01252.x, 2005.

Bond-Lamberty, B., and Gower, S. T.: Decomposition and fragmentation of coarse woody debris: Re-visiting a boreal black spruce chronosequence, Ecosystems, 11, 831-840, 10.1007/s10021-008-9163-y, 2008.

Bond-Lamberty, B., Peckham, S. D., Gower, S. T., and Ewers, B. E.: Effects of fire on regional 725   evapotranspiration in the central Canadian boreal forest, Global Change Biol, 15, 1242-1254, 10.1111/j.1365-2486.2008.01776.x, 2009.

Bowman, D. M., Balch, J. K., Artaxo, P., Bond, W. J., Carlson, J. M., Cochrane, M. A., D'Antonio, C. M., Defries, R. S., Doyle, J. C., Harrison, S. P., Johnston, F. H., Keeley, J. E., Krawchuk, M. A., Kull, C. A., Marston, J. B., Moritz, M. A., Prentice, I. C., Roos, C. I., Scott, A. C., 730   Swetnam, T. W., van der Werf, G. R., and Pyne, S. J.: Fire in the Earth system, Science, 324, 481-484, 10.1126/science.1163886, 2009.

Burton, C., Betts, R., Cardoso, M., Feldpausch, T. R., Harper, A., Jones, C. D., Kelley, D. I., Robertson, E., and Wiltshire, A.: Representation of fire, land-use change and vegetation

dynamics in the Joint UK Land Environment Simulator vn4.9 (JULES), Geosci Model Dev, 12, 179-193, 10.5194/gmd-12-179-2019, 2019.

Chambers, S. D., and Chapin, F. S.: Fire effects on surface-atmosphere energy exchange in Alaskan black spruce ecosystems: Implications for feedbacks to regional climate, J Geophys Res-Atmos, 108, 10.1029/2001jd000530, 2002.

Chuvieco, E., Yue, C., Heil, A., Mouillot, F., Alonso-Canas, I., Padilla, M., Pereira, J. M., Oom, D., and Tansey, K.: A new global burned area product for climate assessment of fire impacts, Global Ecol Biogeogr, 25, 619-629, 10.1111/geb.12440, 2016.

CIESIN: Gridded Population of the World, Version 3 (GPWv3): Population Count Grid. Palisades, NY: NASA Socioeconomic Data and Applications Center (SEDAC), 2014.

Cox, P. M.: Description of the TRIFFID dynamic global vegetation model, 2001.

de Oliveira, C. P., Francelino, M. R., Daher, M., de Araujo, E. J. G., Sanches, L. D., de Andrade, K. D. C., and de Campos, J. S. N.: Estimation of the aboveground biomass and carbon stocks in open Brazilian Savannah developed on sandy soils, Carbon Balance and Management, 14, 2019.

De Sales, F., Xue, Y. K., and Okin, G. S.: Impact of burned areas on the northern African seasonal climate from the perspective of regional modeling, Climate Dynamics, 47, 3393-3413, 10.1007/s00382-015-2522-4, 2016.

Devine, A. P., Stott, I., McDonald, R. A., and Maclean, I. M. D.: Woody cover in wet and dry African savannas after six decades of experimental fires, J Ecol, 103, 473-478, 2015.

Dunin, F.: Run-off and drainage from grassland catchments, 1987.

Forkel, M., Andela, N., Harrison, S. P., Lasslop, G., van Marle, M., Chuvieco, E., Dorigo, W., Forrest, M., Hantson, S., Heil, A., Li, F., Melton, J., Sitch, S., Yue, C., and Arneth, A.: Emergent relationships with respect to burned area in global satellite observations and fire-enabled vegetation models, Biogeosciences, 16, 57-76, 10.5194/bg-16-57-2019, 2019.

Furley, P. A., Rees, R. M., Ryan, C. M., and Saiz, G.: Savanna burning and the assessment of long-term fire experiments with particular reference to Zimbabwe, Prog Phys Geog, 32, 611-634, 2008.

Gholz, H. L., and Clark, K. L.: Energy exchange across a chronosequence of slash pine forests in Florida, Agr Forest Meteorol, 112, 87-102, 2002.

Giglio, L., Csiszar, I., and Justice, C. O.: Global distribution and seasonality of active fires as observed with the Terra and Aqua Moderate Resolution Imaging Spectroradiometer (MODIS) sensors, J Geophys Res-Biogeo, 111, 10.1029/2005jg000142, 2006.

Giglio, L., Randerson, J. T., and van der Werf, G. R.: Analysis of daily, monthly, and annual burned area using the fourth-generation global fire emissions database (GFED4), J Geophys Res-Biogeo, 118, 317-328, 10.1002/jgrg.20042, 2013.

Giglio, L., Boschetti, L., Roy, D. P., Humber, M. L., and Justice, C. O.: The Collection 6 MODIS burned area mapping algorithm and product, Remote Sens Environ, 217, 72-85, 10.1016/j.rse.2018.08.005, 2018.

Goldewijk, K. K., Beusen, A., and Janssen, P.: Long-term dynamic modeling of global population and built-up area in a spatially explicit way: HYDE 3.1, Holocene, 20, 565-573, 2010.

Hamilton, D. S., Hantson, S., Scott, C. E., Kaplan, J. O., Pringle, K. J., Nieradzik, L. P., Rap, A., Folberth, G. A., Spracklen, D. V., and Carslaw, K. S.: Reassessment of pre-industrial fire emissions strongly affects anthropogenic aerosol forcing, Nat Commun, 9, 10.1038/s41467-018-05592-9, 2018.

Hantson, S., Kelley, D. I., Arneth, A., Harrison, S. P., Archibald, S., Bachelet, D., Forrest, M.,
780   Hickler, T., Lasslop, G., Li, F., Mangeon, S., Melton, J. R., Nieradzik, L., Rabin, S. S.,
            Prentice, I. C., Sheehan, T., Sitch, S., Teckentrup, L., Voulgarakis, A., and Yue, C.:
            Quantitative assessment of fire and vegetation properties in historical simulations with fire-
            enabled vegetation models from the Fire Model Intercomparison Project, Geosci. Model
            Dev. Discuss., 2020, 1-25, 10.5194/gmd-2019-261, 2020.
785   Harper, A. B., Cox, P. M., Friedlingstein, P., Wiltshire, A. J., Jones, C. D., Sitch, S., Mercado, L.
            M., Groenendijk, M., Robertson, E., Kattge, J., Bonisch, G., Atkin, O. K., Bahn, M.,
            Cornelissen, J., Niinemets, U., Onipchenko, V., Penuelas, J., Poorter, L., Reich, P. B.,
            Soudzilovskaia, N. A., and van Bodegom, P.: Improved representation of plant functional
            types and physiology in the Joint UK Land Environment Simulator (JULES v4.2) using
790   plant trait information, Geosci Model Dev, 9, 2415-2440, 10.5194/gmd-9-2415-2016, 2016.
       Higgins, S. I., Bond, W. J., February, E. C., Bronn, A., Euston-Brown, D. I. W., Enslin, B.,
            Govender, N., Rademan, L., O'Regan, S., Potgieter, A. L. F., Scheiter, S., Sowry, R.,
            Trollope, L., and Trollope, W. S. W.: Effects of four decades of fire manipulation on woody
            vegetation structure in savanna, Ecology, 88, 1119-1125, 2007.
795   Huang, H., Xue, Y., Chilukoti, N., Liu, Y., Chen, G., and Diallo, I.: Assessing global and regional
            effects of reconstructed land use and land cover change on climate since 1950 using a
            coupled land-atmosphere-ocean model, J Climate, 2020. 1-58, 10.1175/JCLI-D-20-0108.1,
            2020.
       Jiang, Y. Q., Lu, Z., Liu, X. H., Qian, Y., Zhang, K., Wang, Y. H., and Yang, X. Q.: Impacts of
800   global open-fire aerosols on direct radiative, cloud and surface-albedo effects simulated
            with CAM5, Atmos Chem Phys, 16, 14805-14824, 10.5194/acp-16-14805-2016, 2016.
       Johnston, F. H., Henderson, S. B., Chen, Y., Randerson, J. T., Marlier, M., DeFries, R. S., Kinney,
            P., Bowman, D. M. J. S., and Brauer, M.: Estimated Global Mortality Attributable to
            Smoke from Landscape Fires, Environ Health Persp, 120, 695-701, 10.1289/ehp.1104422,
805   2012.
       Jung, M., Reichstein, M., Margolis, H. A., Cescatti, A., Richardson, A. D., Arain, M. A., Arneth,
            A., Bernhofer, C., Bonal, D., Chen, J. Q., Gianelle, D., Gobron, N., Kiely, G., Kutsch, W.,
            Lasslop, G., Law, B. E., Lindroth, A., Merbold, L., Montagnani, L., Moors, E. J., Papale,
            D., Sottocornola, M., Vaccari, F., and Williams, C.: Global patterns of land-atmosphere
810   fluxes of carbon dioxide, latent heat, and sensible heat derived from eddy covariance,
            satellite, and meteorological observations, J Geophys Res-Biogeo, 116, 2011.
       Kloster, S., Mahowald, N. M., Randerson, J. T., and Lawrence, P. J.: The impacts of climate, land
            use, and demography on fires during the 21st century simulated by CLM-CN,
            Biogeosciences, 9, 509-525, 2012.
815   Knorr, W., Jiang, L., and Arneth, A.: Climate, CO2 and human population impacts on global
            wildfire emissions, Biogeosciences, 13, 267-282, 10.5194/bg-13-267-2016, 2016.
       Langford, K. J.: Change in Yield of Water Following a Bushfire in a Forest of Eucalyptus Regnans,
            J Hydrol, 29, 87-114, 1976.
       Lasslop, G., Thonicke, K., and Kloster, S.: SPITFIRE within the MPI Earth system model: Model
820   development and evaluation, Journal of Advances in Modeling Earth Systems, 6, 740-755,
            10.1002/2013ms000284, 2014.
       Lasslop, G., Hantson, S., Harrison, S. P., Bachelet, D., Burton, C., Forkel, M., . . . Sitch, S.: Global
            ecosystems and fire: Multi-model assessment of fire-induced tree-cover and carbon storage
            reduction, Global Change Biol, n/a, 10.1111/gcb.15160, 2020.

Lawrence, D. M., Fisher, R. A., Koven, C. D., Oleson, K. W., Swenson, S. C., Bonan, G., Collier, N., Ghimire, B., van Kampenhout, L., Kennedy, D., Kluzek, E., Lawrence, P. J., Li, F., Li, H. Y., Lombardozzi, D., Riley, W. J., Sacks, W. J., Shi, M. J., Vertenstein, M., Wieder, W. R., Xu, C. G., Ali, A. A., Badger, A. M., Bisht, G., van den Broeke, M., Brunke, M. A., Burns, S. P., Buzan, J., Clark, M., Craig, A., Dahlin, K., Drewniak, B., Fisher, J. B., Flanner, M., Fox, A. M., Gentine, P., Hoffman, F., Keppel-Aleks, G., Knox, R., Kumar, S., Lenaerts, J., Leung, L. R., Lipscomb, W. H., Lu, Y. Q., Pandey, A., Pelletier, J. D., Perket, J., Randerson, J. T., Ricciuto, D. M., Sanderson, B. M., Slater, A., Subin, Z. M., Tang, J. Y., Thomas, R. Q., Martin, M. V., and Zeng, X. B.: The Community Land Model Version 5: Description of New Features, Benchmarking, and Impact of Forcing Uncertainty, Journal of Advances in Modeling Earth Systems, 11, 4245-4287, 10.1029/2018ms001583, 2019.

Li, F., and Lawrence, D. M.: Role of Fire in the Global Land Water Budget during the Twentieth Century due to Changing Ecosystems, J Climate, 30, 1893-1908, 10.1175/Jcli-D-16-0460.1, 2017.

Li, F., Zeng, X. D., and Levis, S.: A process-based fire parameterization of intermediate complexity in a Dynamic Global Vegetation Model, Biogeosciences, 9, 2761-2780, 10.5194/bg-9-2761-2012, 2012.

Li, F., Levis, S., and Ward, D. S.: Quantifying the role of fire in the Earth system - Part 1: Improved global fire modeling in the Community Earth System Model (CESM1), Biogeosciences, 10, 2293-2314, 10.5194/bg-10-2293-2013, 2013.

Li, F., Bond-Lamberty, B., and Levis, S.: Quantifying the role of fire in the Earth system - Part 2: Impact on the net carbon balance of global terrestrial ecosystems for the 20th century, Biogeosciences, 11, 1345-1360, 10.5194/bg-11-1345-2014, 2014.

Li, F., Lawrence, D. M., and Bond-Lamberty, B.: Impact of fire on global land surface air temperature and energy budget for the 20th century due to changes within ecosystems (vol 12, 044014, 2017), Environ Res Lett, 12, 10.1088/1748-9326/aa727f, 2017.

Li, F., Val Martin, M., Hantson, S., Andreae, M. O., Arneth, A., Lasslop, G., Yue, C., Bachelet, D., Forrest, M., Kaiser, J. W., Kluzek, E., Liu, X., Melton, J. R., Ward, D. S., Darmenov, A., Hickler, T., Ichoku, C., Magi, B. I., Sitch, S., van der Werf, G. R., and Wiedinmyer, C.: Historical (1700-2012) Global Multi-model Estimates of the Fire Emissions from the Fire Modeling Intercomparison Project (FireMIP), Atmos. Chem. Phys., 19, 12545–12567, https://doi.org/10.5194/acp-19-12545-2019, 2019.

Liu, H. P., Randerson, J. T., Lindfors, J., and Chapin, F. S.: Changes in the surface energy budget after fire in boreal ecosystems of interior Alaska: An annual perspective, J Geophys Res-Atmos, 110, 10.1029/2004jd005158, 2005.

Liu, Y., Guo, W. D., and Song, Y. M.: Estimation of key surface parameters in semi-arid region and their impacts on improvement of surface fluxes simulation, Sci China Earth Sci, 59, 307-319, 10.1007/s11430-015-5140-4, 2016.

Liu, Y., Xue, Y. K., MacDonald, G., Cox, P., and Zhang, Z. Q.: Global vegetation variability and its response to elevated CO2, global warming, and climate variability - a study using the offline SSiB4/TRIFFID model and satellite data, Earth Syst Dynam, 10, 9-29, 2019.

Melton, J. R., and Arora, V. K.: Competition between plant functional types in the Canadian Terrestrial Ecosystem Model (CTEM) v.2.0, Geosci Model Dev, 9, 323-361, 2016.

Moreira, A. G.: Effects of fire protection on savanna structure in Central Brazil, Journal of Biogeography, 27, 1021-1029, 2000.

870   Oleson, K., Lawrence, D., Bonan, G., Drewniak, B., Huang, M., Koven, C., Levis, S., Li, F., Riley, W., and Subin, Z.: Technical Description of version 4.5 of the Community Land Model (CLM)(NCAR Technical Note No. NCAR/TN-503+ STR). Citeseer, National Center for Atmospheric Research, PO Box, 3000, 2013.

Pan, Y., Birdsey, R. A., Fang, J., Houghton, R., Kauppi, P. E., Kurz, W. A., . . . Canadell, J. G.: A
875   large and persistent carbon sink in the world's forests, Science, 333, 988-993, 2011.

Parton, W. J., Ojima, D. S., Cole, C. V., and Schimel, D. S.: A General Model for Soil Organic Matter Dynamics - Sensitivity to Litter Chemistry, Texture and Management, Sssa Spec Publ, 147-167, 1994.

Pechony, O., and Shindell, D. T.: Fire parameterization on a global scale, J Geophys Res-Atmos,
880   114, 10.1029/2009jd011927, 2009.

Pfeiffer, M., and Kaplan, J. O.: SPITFIRE-2: an improved fire module for Dynamic Global Vegetation Models, Universitätsbibliothek Johann Christian Senckenberg, 2012.

Pfeiffer, M., Spessa, A., and Kaplan, J. O.: A model for global biomass burning in preindustrial time: LPJ-LMfire (v1.0), Geosci Model Dev, 6, 643-685, 10.5194/gmd-6-643-2013, 2013.

885   Piao, S. L., Sitch, S., Ciais, P., Friedlingstein, P., Peylin, P., Wang, X. H., Ahlstrom, A., Anav, A., Canadell, J. G., Cong, N., Huntingford, C., Jung, M., Levis, S., Levy, P. E., Li, J. S., Lin, X., Lomas, M. R., Lu, M., Luo, Y. Q., Ma, Y. C., Myneni, R. B., Poulter, B., Sun, Z. Z., Wang, T., Viovy, N., Zaehle, S., and Zeng, N.: Evaluation of terrestrial carbon cycle models for their response to climate variability and to CO2 trends, Global Change Biol, 19,
890   2117-2132, 10.1111/gcb.12187, 2013.

Poulter, B., Cadule, P., Cheiney, A., Ciais, P., Hodson, E., Peylin, P., Plummer, S., Spessa, A., Saatchi, S., Yue, C., and Zimmermann, N. E.: Sensitivity of global terrestrial carbon cycle dynamics to variability in satellite-observed burned area, Global Biogeochem Cy, 29, 207-222, 2015.

895   Prentice, S., and Mackerras, D.: The ratio of cloud to cloud-ground lightning flashes in thunderstorms, J Appl Meteorol, 16, 545-550, 1977.

Rabin, S. S., Ward, D. S., Malyshev, S. L., Magi, B. I., Shevliakova, E., and Pacala, S. W.: A fire model with distinct crop, pasture, and non-agricultural burning: use of new data and a model-fitting algorithm for FINAL.1, Geosci Model Dev, 11, 815-842, 10.5194/gmd-11-
900   815-2018, 2018.

Randerson, J. T., Chen, Y., van der Werf, G. R., Rogers, B. M., and Morton, D. C.: Global burned area and biomass burning emissions from small fires, J Geophys Res-Biogeo, 117, 10.1029/2012jg002128, 2012.

Ricciuto, D., Sargsyan, K., and Thornton, P.: The Impact of Parametric Uncertainties on
905   Biogeochemistry in the E3SM Land Model, Journal of Advances in Modeling Earth Systems, 10, 297-319, 10.1002/2017ms000962, 2018.

Rogers, B. M., Randerson, J. T., and Bonan, G. B.: High-latitude cooling associated with landscape changes from North American boreal forest fires, Biogeosciences, 10, 699-718, 10.5194/bg-10-699-2013, 2013.

910   Saha, M. V., Scanlon, T. M., and D'Odorico, P.: Suppression of rainfall by fires in African drylands, Geophys Res Lett, 43, 8527-8533, 10.1002/2016gl069855, 2016.

Sankaran, M., Hanan, N. P., Scholes, R. J., Ratnam, J., Augustine, D. J., Cade, B. S., Gignoux, J., Higgins, S. I., Le Roux, X., Ludwig, F., Ardo, J., Banyikwa, F., Bronn, A., Bucini, G., Caylor, K. K., Coughenour, M. B., Diouf, A., Ekaya, W., Feral, C. J., February, E. C., Frost,
915   P. G. H., Hiernaux, P., Hrabar, H., Metzger, K. L., Prins, H. H. T., Ringrose, S., Sea, W.,

Tews, J., Worden, J., and Zambatis, N.: Determinants of woody cover in African savannas, Nature, 438, 846-849, 2005.

Santos, A. J. B., Silva, G. T. D. A., Miranda, H. S., Miranda, A. C., and Lloyd, J.: Effects of fire on surface carbon, energy and water vapour fluxes over campo sujo savanna in central Brazil, Funct Ecol, 17, 711-719, 2003.

Scholes, R. J., Ward, D. E., and Justice, C. O.: Emissions of trace gases and aerosol particles due to vegetation burning in southern hemisphere Africa, J Geophys Res-Atmos, 101, 23677-23682, Doi 10.1029/95jd02049, 1996.

Schulze, E. D., Kelliher, F. M., Korner, C., Lloyd, J., and Leuning, R.: Relationships among Maximum Stomatal Conductance, Ecosystem Surface Conductance, Carbon Assimilation Rate, and Plant Nitrogen Nutrition - a Global Ecology Scaling Exercise, Annu Rev Ecol Syst, 25, 629-+, DOI 10.1146/annurev.es.25.110194.003213, 1994.

Seo, H., and Kim, Y.: Interactive impacts of fire and vegetation dynamics on global carbon and water budget using Community Land Model version 4.5, Geosci Model Dev, 12, 457-472, 10.5194/gmd-12-457-2019, 2019.

Shackleton, C., and Scholes, R. J.: Impact of fire frequency on woody community structure and soil nutrients in the Kruger National Park, Koedoe, 43, 75-81, 2000.

Sheffield, J., Goteti, G., and Wood, E. F.: Development of a 50-year high-resolution global dataset of meteorological forcings for land surface modeling, J Climate, 19, 3088-3111, Doi 10.1175/Jcli3790.1, 2006.

Shinoda, M., and Yamaguchi, Y.: Influence of soil moisture anomaly on temperature in the Sahel: A comparison between wet and dry decades, J Hydrometeorol, 4, 437-447, Doi 10.1175/1525-7541(2003)4<437:Iosmao>2.0.Co;2, 2003.

Smit, I. P. J., Asner, G. P., Govender, N., Kennedy-Bowdoin, T., Knapp, D. E., and Jacobson, J.: Effects of fire on woody vegetation structure in African savanna, Ecol Appl, 20, 1865-1875, 2010.

Sousa, W. P.: The Role of Disturbance in Natural Communities, Annu Rev Ecol Syst, 15, 353-391, DOI 10.1146/annurev.es.15.110184.002033, 1984.

Sun, G., Noormets, A., Gavazzi, M. J., McNulty, S. G., Chen, J., Domec, J. C., King, J. S., Amatya, D. M., and Skaggs, R. W.: Energy and water balance of two contrasting loblolly pine plantations on the lower coastal plain of North Carolina, USA, Forest Ecol Manag, 259, 1299-1310, 2010.

Teckentrup, L., Harrison, S. P., Hantson, S., Heil, A., Melton, J. R., Forrest, M., Li, F., Yue, C., Arneth, A., Hickler, T., Sitch, S., and Lasslop, G.: Response of simulated burned area to historical changes in environmental and anthropogenic factors: a comparison of seven fire models, Biogeosciences, 16, 3883-3910, 2019.

Thonicke, K., Venevsky, S., Sitch, S., and Cramer, W.: The role of fire disturbance for global vegetation dynamics: coupling fire into a Dynamic Global Vegetation Model, Global Ecol Biogeogr, 10, 661-677, DOI 10.1046/j.1466-822x.2001.00175.x, 2001.

Thonicke, K., Spessa, A., Prentice, I. C., Harrison, S. P., Dong, L., and Carmona-Moreno, C.: The influence of vegetation, fire spread and fire behaviour on biomass burning and trace gas emissions: results from a process-based model (vol 7, pg 1991, 2010), Biogeosciences, 7, 2191-2191, 10.5194/bg-7-2191-2010, 2010.

van der Werf, G. R., Randerson, J. T., Giglio, L., Collatz, G. J., Kasibhatla, P. S., and Arellano Jr, A. F.: Interannual variability in global biomass burning emissions from 1997 to 2004, Atmos Chem Phys, 6, 3423-3441, 2006.

van der Werf, G. R., Randerson, J. T., Giglio, L., Collatz, G. J., Mu, M., Kasibhatla, P. S., Morton, D. C., DeFries, R. S., Jin, Y., and van Leeuwen, T. T.: Global fire emissions and the contribution of deforestation, savanna, forest, agricultural, and peat fires (1997-2009), Atmos Chem Phys, 10, 11707-11735, 2010.

van der Werf, G. R., Randerson, J. T., Giglio, L., van Leeuwen, T. T., Chen, Y., Rogers, B. M., Mu, M. Q., van Marle, M. J. E., Morton, D. C., Collatz, G. J., Yokelson, R. J., and Kasibhatla, P. S.: Global fire emissions estimates during 1997-2016, Earth Syst Sci Data, 9, 697-720, 2017.

van Marle, M. J. E., Kloster, S., Magi, B. I., Marlon, J. R., Daniau, A. L., Field, R. D., Arneth, A., Forrest, M., Hantson, S., Kehrwald, N. M., Knorr, W., Lasslop, G., Li, F., Mangeon, S., Yue, C., Kaiser, J. W., and van der Werf, G. R.: Historic global biomass burning emissions for CMIP6 (BB4CMIP) based on merging satellite observations with proxies and fire models (1750-2015), Geosci Model Dev, 10, 3329-3357, 10.5194/gmd-10-3329-2017, 2017.

van Vuuren, D. P., Lucas, P. L., and Hilderink, H.: Downscaling drivers of global environmental change: Enabling use of global SRES scenarios at the national and grid levels, Global Environ Chang, 17, 114-130, 2007.

van Wilgen, B. W., Govender, N., and Biggs, H. C.: The contribution of fire research to fire management: a critical review of a long-term experiment in the Kruger National Park, South Africa, Int J Wildland Fire, 16, 519-530, 2007.

Venevsky, S., Thonicke, K., Sitch, S., and Cramer, W.: Simulating fire regimes in human-dominated ecosystems: Iberian Peninsula case study, Global Change Biol, 8, 984-998, DOI 10.1046/j.1365-2486.2002.00528.x, 2002.

Venevsky, S., Le Page, Y., Pereira, J. M. C., and Wu, C.: Analysis fire patterns and drivers with a global SEVER-FIRE v1.0 model incorporated into dynamic global vegetation model and satellite and on-ground observations, Geosci. Model Dev., 12, 89-110, 10.5194/gmd-12-89-2019, 2019.

Ward, D. S., Kloster, S., Mahowald, N. M., Rogers, B. M., Randerson, J. T., and Hess, P. G.: The changing radiative forcing of fires: global model estimates for past, present and future, Atmos Chem Phys, 12, 10857-10886, 10.5194/acp-12-10857-2012, 2012.

Ward, D. S., Shevliakova, E., Malyshev, S., and Rabin, S.: Trends and Variability of Global Fire Emissions Due To Historical Anthropogenic Activities, Global Biogeochem Cy, 32, 122-142, 10.1002/2017gb005787, 2018.

Xia, X. G., Zong, X. M., and Sun, L.: Exceptionally active agricultural fire season in mid-eastern China in June 2012 and its impact on the atmospheric environment, J Geophys Res-Atmos, 118, 9889-9900, 10.1002/jgrd.50770, 2013.

Xue, Y., Sellers, P. J., Kinter, J. L., and Shukla, J.: A Simplified Biosphere Model for Global Climate Studies, J Climate, 4, 345-364, 10.1175/1520-0442(1991)004<0345:asbmfg>2.0.co;2, 1991.

Yang, J., Tian, H. Q., Tao, B., Ren, W., Kush, J., Liu, Y. Q., and Wang, Y. H.: Spatial and temporal patterns of global burned area in response to anthropogenic and environmental factors: Reconstructing global fire history for the 20th and early 21st centuries, J Geophys Res-Biogeo, 119, 249-263, 10.1002/2013jg002532, 2014.

Yang, J., Tian, H. Q., Tao, B., Ren, W., Pan, S. F., Liu, Y. Q., and Wang, Y. H.: A growing importance of large fires in conterminous United States during 1984-2012, J Geophys Res-Biogeo, 120, 2625-2640, 10.1002/2015jg002965, 2015.

Yue, C., Ciais, P., Cadule, P., Thonicke, K., Archibald, S., Poulter, B., . . . Viovy, N.: Modelling the role of fires in the terrestrial carbon balance by incorporating SPITFIRE into the global vegetation model ORCHIDEE - Part 1: simulating historical global burned area and fire regimes, Geosci Model Dev, 7, 2747-2767, 10.5194/gmd-7-2747-2014, 2014.

Yue, C., Ciais, P., Cadule, P., Thonicke, K., and van Leeuwen, T. T.: Modelling the role of fires in the terrestrial carbon balance by incorporating SPITFIRE into the global vegetation model ORCHIDEE - Part 2: Carbon emissions and the role of fires in the global carbon balance, Geosci Model Dev, 8, 1321-1338, 10.5194/gmd-8-1321-2015, 2015.

Zeng, F. W., Koster, R. D., Lee, E., Follette-Cook, M. B., Weir, B., Colarco, P. R., Ott, L., and Poulter, B.: Use of CLM Carbon Dynamics in the Land Component of the NASA GMAO Earth System Model, 2019.

Zeng, X. D., Li, F., and Song, X.: Development of the IAP Dynamic Global Vegetation Model, Advances in Atmospheric Sciences, 31, 505-514, 10.1007/s00376-013-3155-3, 2014.

Zhan, X. W., Xue, Y. K., and Collatz, G. J.: An analytical approach for estimating CO_2 and heat fluxes over the Amazonian region, Ecol Model, 162, 97-117, 2003.

Zhang, Z., Xue, Y., MacDonald, G., Cox, P. M., and Collatz, G. J.: Investigation of North American vegetation variability under recent climate: A study using the SSiB4/TRIFFID biophysical/dynamic vegetation model, Journal of Geophysical Research: Atmospheres, 120, 1300-1321, 2015.

Zheng, B., Chevallier, F., Yin, Y., Ciais, P., Fortems-Cheiney, A., Deeter, M. N., . . . Zhao, Y. H.: Global atmospheric carbon monoxide budget 2000-2017 inferred from multi-species atmospheric inversions, Earth Syst Sci Data, 11, 1411-1436, 10.5194/essd-11-1411-2019, 2019.

Zou, Y. F., Wang, Y. H., Qian, Y., Tian, H. Q., Yang, J., and Alvarado, E.: Using CESM-RESFire to understand climate-fire-ecosystem interactions and the implications for decadal climate variability, Atmos Chem Phys, 20, 995-1020, 10.5194/acp-20-995-2020, 2020.